

# Auto-encoding brain networks with applications to analyzing large-scale brain imaging datasets

Meimei Liu\*, Zhengwu Zhang†, David B. Dunson‡

## Abstract

There has been huge interest in studying human brain connectomes inferred from different imaging modalities and exploring their relationship with human traits, such as cognition. Brain connectomes are usually represented as networks, with nodes corresponding to different regions of interest (ROIs) and edges to connection strengths between ROIs. Due to the high-dimensionality and non-Euclidean nature of networks, it is challenging to depict their population distribution and relate them to human traits. Current approaches focus on summarizing the network using either pre-specified topological features or principal components analysis (PCA). In this paper, building on recent advances in deep learning, we develop a nonlinear latent factor model to characterize the population distribution of brain graphs and infer the relationships between brain structural connectomes and human traits. We refer to our method as Graph AuTo-Encoding (GATE). We applied GATE to two large-scale brain imaging datasets, the Adolescent Brain Cognitive Development (ABCD) study and the Human Connectome Project (HCP) for adults, to understand the structural brain connectome and its relationship with cognition. Numerical results demonstrate huge advantages of GATE over competitors in terms of prediction accuracy, statistical inference and computing efficiency. We found that structural connectomes have a stronger association with a wide range of human cognitive traits than was apparent using previous approaches.

**Keywords:** Brain networks; Non-linear factor analysis; Graph CNN; Neuroscience; Replicated networks; Variational Auto-encoder.

## 1 Introduction

Understanding the brain connectome and how it relates to human traits and various clinical variables has drawn huge attention [Park and Friston \(2013\)](#); [Fornito et al. \(2013\)](#); [Craddock et al. \(2013\)](#);

---

\*Virginia Tech, E-mail: meimeiliu@vt.edu.

†The University of North Carolina at Chapel Hill, E-mail:zhengwu\_zhang@unc.edu

‡Duke University E-mail: dunson@duke.edu. We acknowledge the funding from NIH R01-MH118927 and the Alibaba funding support.

Jones et al. (2013). This has motivated large neuroimaging studies with thousands of subjects, such as the UK Biobank (UKB) Miller et al. (2016), the Adolescent Brain Cognitive Development (ABCD) study Casey et al. (2018), and the Human Connectome Project (HCP) Van Essen et al. (2013). Through these studies, there have been dramatic improvements in the ability to reconstruct brain connectomes thanks to advanced hardware Glasser et al. (2016), novel image acquisition protocols Glasser et al. (2016); Tuch (2004), and new reconstruction algorithms Zhang et al. (2018); Smith et al. (2012). In this paper, we are particularly interested in diffusion magnetic resonance imaging (dMRI), which is a commonly used technique that measures the movement of water molecules along major fiber bundles in white matter (WM) fiber tracts, enabling reconstruction of individual-level microstructural brain networks delineating anatomical connections between brain regions. This paper aims at developing advanced analysis methods for the brain structural connectomes recovered from diffusion MRI data.

Let  $A_i$  represent the structural connectivity recovered from subject  $i$ , with element  $A_{i[uv]}$  measuring white matter connections between brain regions  $u$  and  $v$ . Using  $n$  individual brain networks, we are interested in (a) appropriately summarizing each individual brain network in a parsimonious manner, isolating unique features of the network without discarding valuable information, (b) inferring relationships between brain networks and human traits, and (c) characterizing variation across individuals in their network structure.

There are existing methods that are relevant to these goals. Based on a latent space characterization, Durante et al. (2017) proposed a random effects model to represent the population distribution of brain networks. Their Bayesian approach clusters individuals based on brain structure and allows inferences on group differences Durante and Dunson (2018). Potential disadvantages include the highly computationally intensive implementation and coarse characterization of individual differences based on clustering. There is also literature on PCA-style approaches. One possibility is to simply stack the adjacency matrices  $A_i$  for individuals  $i = 1, \dots, n$  into a tensor, and then apply tensor PCA and its variants to get summary scores of networks Zhang et al. (2019); Zhang and Dunson (2019). These scores are treated as brain network surrogates in subsequent analyses, e.g., relating brain networks to human traits Zhang et al. (2019). Tensor PCA is relatively efficient computationally while providing a simple low-dimensional summary of an individual’s brain structure, but it is linear, which may limit ability to parsimoniously represent brain networks. An alternative is graph representations based on geometric deep learning. Kipf and Welling (2017), Hamilton et al. (2017) proposed graph convolutional networks (GCN) that use structure information in learning a low-dimensional feature representation for each node in a graph. Kawahara et al. (2017), Ktena et al. (2018) applied GCN to functional brain connectomes for classification and similarity ranking. Advanced graph embeddings for structural brain connectomes are still lacking.

A major motivation of this article is to develop a nonlinear latent factor modeling approach that provides a characterization of the population distribution of brain graphs, while also outputting a low-dimensional vector of features that can be used to summarize an individual’s graph, facilitating prediction and inference on relationships between connectomes and human traits. With this motivation, we are particularly intrigued by deep neural networks for non-linear dimension reduction. Generative algorithms, such as Variational Auto-Encoders (VAEs) [Kingma and Welling \(2014\)](#); [Rezende et al. \(2014\)](#), have proven successful in representing images via low dimensional latent variables. VAEs model the population distribution of image data through a simple distribution for the latent variables combined with a complex non-linear mapping function. A key to the success of such methods is the use of convolutional operators to encode symmetries often present in images. However, structural brain networks have a fundamentally different geometric structure, and such methods cannot be employed directly. We develop a model-based variational **Graph Auto-Encoder** (GATE) for brain connectome analysis. Our main contributions can be summarized as follows.

First, GATE learns the embedding and the population distribution of brain connectomes simultaneously. This is achieved by: 1) a nonlinear latent factor model to obtain a low-dimensional representation  $z_i$  of brain network  $A_i$ ; and 2) a hierarchical generative model designed to learn the conditional distribution  $p(A_i|z_i)$  so that one can accurately reconstruct the brain network from the latent embedding. We model each cell  $A_{i[uv]}$  in  $A_i$  using a latent space model [Hoff et al. \(2002\)](#), with the latent coordinates of the regions  $u$  and  $v$  varying as a nonlinear function of the individual-specific features  $z_i$ . This step involves a novel graph convolutional network that relies on intrinsic locality of the brain networks to propagate node-specific  $k$ -nearest neighbor information.

Second, we extend GATE to relate human phenotypes to brain structural connectivity, which we refer to as **regression with GATE** (reGATE). reGATE is a supervised embedding method that simultaneously learns the population distribution of brain networks, network embeddings and a predictive model for human traits. Although there has been some work integrating regression models and VAEs, the focus has been on multi-stage approaches; e.g., see [Yoo et al. \(2017\)](#) as an example. reGATE can generate from the population distribution of brain networks conditionally on the value of a human trait. This provides invaluable information about how traits and brain networks are associated, while characterizing variation across individuals. We further draw inference on selected network summary measures of interest, such as network density and average path length, to understand how these properties are distributed depending on human traits.

We apply GATE and reGATE to brain connectomes from ABCD and HCP, and find strong relationships between structural connectomes and cognition traits in both datasets. ReGATE shows superior performance in predicting the relationship between cognition and brain connectomes, particularly when trained with data from large numbers of individuals. For example, using more

than five thousand brain scans in the ABCD study, reGATE improves prediction of cognitive traits by 30% – 40% compared with existing competitors. Through detailed inference based on reGATE, we show that individuals with high levels of cognitive traits tend to have denser connections between hemispheres, higher overall network density and lower average path length. Such network summary measures have higher variability across the children evaluated in ABCD compared with adults in HCP.

## 2 Methods

### 2.1 Brain Imaging Datasets and Structural Connectome Extraction

We focus on two large datasets in this paper: the Adolescent Brain Cognitive Development (ABCD) dataset and the Human Connectome Project (HCP) dataset.

**ABCD dataset:** The ABCD study in the United States focuses on tracking brain development from childhood through adolescence to understand biological and environmental factors that can affect the brain’s developmental trajectory. The research consortium consists of 21 research sites across the country, and invited 11,878 9-10 year old children to participate. Researchers track their biological and behavioral development through adolescence into young adulthood. The dataset can be downloaded from NIH Data Archive (NDA, <https://nda.nih.gov>). The imaging protocol is harmonized for three types of 3T scanners: Siemens Prisma, General Electric (GE) 750, and Philips. We downloaded the structural T1 MRI and diffusion MRI (dMRI) data for 5253 subjects from the ABCD 2.0 release in NDA. The structural T1 images were acquired with isotropic resolution of 1 mm<sup>3</sup>. The diffusion MRI images were obtained based on imaging parameters: 1.7 mm<sup>3</sup> resolution, four different b-values ( $b = 500, 1000, 2000, 3000$ ) and 96 diffusion directions. There are 6 directions at  $b = 500$ , 15 directions at  $b = 1000$ , 15 directions at  $b = 2000$ , and 60 directions at  $b = 3000$ . Multiband factor 3 is used for dMRI acceleration. See [Casey et al. \(2018\)](#) for more details about data acquisition and preprocessing of the ABCD data.

**HCP dataset:** The HCP aims at characterizing human brain connectivity in about 1,200 healthy adults to enable detailed comparisons between brain circuits, behavior, and genetics at the level of individual subjects [Van Essen et al. \(2012\)](#). Customized scanners were used to produce high-quality and consistent data to measure brain connectivity. The data containing various traits and MRI data can be easily accessed through <https://db.humanconnectome.org/>.

To obtain structural connectomes, we used a state-of-the-art dMRI data preprocessing framework – population-based structural connectome (PSC) mapping ([Zhang et al. \(2018\)](#)). PSC uses a reproducible probabilistic tractography algorithm ([Girard et al. \(2014\)](#); [Maier-Hein et al. \(2017\)](#)) to generate whole-brain tractography. PSC borrows anatomical information from high-resolution T1

images to reduce bias in the reconstruction of tractography. We used the Desikan–Killiany atlas (Desikan et al. (2006)) to define the brain regions of interest (ROIs) corresponding to the nodes in the structural connectivity network. The Desikan–Killiany parcellation has 68 cortical surface regions with 34 nodes in each hemisphere. For each pair of ROIs, we extracted the streamlines connecting them. In this process, several procedures were used to increase reproducibility: (1) each gray matter ROI is dilated to include a small portion of white matter region, (2) streamlines connecting multiple ROIs are cut into pieces so that we can extract the correct and complete pathway and (3) outlier streamlines are removed. We use the number of fibers connecting each pair of ROIs as a summary of connectivity in our analyses.

For the ABCD dataset, we processed 5252 subjects using PSC. We focus our analyses on four cognitive traits: (a) picture vocabulary score, (b) oral reading recognition test score, (c) crystallized composite age-corrected standard score, (d) cognition total composite score. The first row in Figure 1 demonstrates the distribution of the four traits. Similarly, for the HCP dataset, we preprocessed 1065 subjects using PSC. We focused on the cognitive traits: (a) picture vocabulary test score, (b) oral reading recognition test score, (c) line orientation - total number correct, and (d) line orientation - total positions off for all trials.

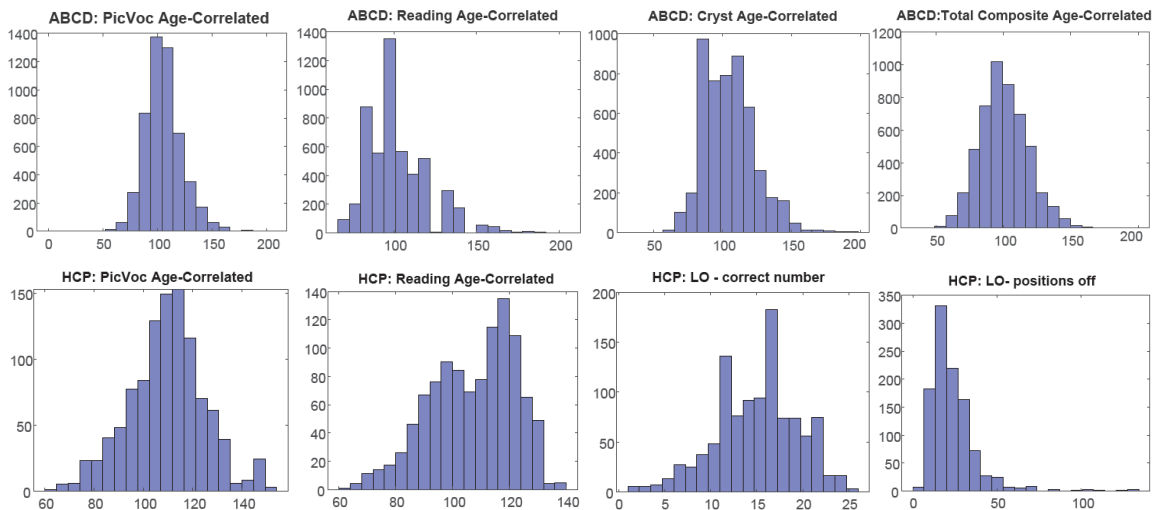


Figure 1: Histograms of cognitive traits. The first row: ABCD study with 5252 subjects involved; from left to right, the traits include picture vocabulary score, oral reading recognition test score, crystallized composite age-corrected standard score, cognition total composite score. The second row: HCP study with 1065 subjects; from left to right: picture vocabulary test score, oral reading recognition test score, line orientation (LO) - total number correct, and line orientation (LO) - total positions off for all trials.

## 2.2 The Graph Auto-Encoder Model

The brain connectome for individual  $i$  is represented as a  $V \times V$  symmetric adjacency matrix  $A_i$ , where  $A_{i[uv]}$  is the count of the number of fibers connecting regions  $u$  and  $v$  in the  $i$ th individual's brain. Using the Desikan atlas, we choose  $V = 68$  ROIs. We let

$$L(A_i) = (A_{i1}, \dots, A_{iV(V-1)/2}) \equiv (A_{i[21]}, A_{i[31]}, \dots, A_{i[V1]}, A_{i[32]}, \dots, A_{i[V2]}, \dots, A_{i[V(V-1)]})$$

denote the lower triangular elements of matrix  $A_i$ . We let  $y_i$  denote the value of a cognitive trait for individual  $i$ . Our goal is to model the population distribution of the  $A_i$ 's and learn the relationship between cognitive traits  $y_i$  and brain structural connectomes  $A_i$ .

### 2.2.1 Latent space model for brain connectomes

Latent space models [Hoff et al. \(2002\)](#) provide a probabilistic framework that assumes the edges in the networks are conditionally independent given their corresponding edge probabilities, with these probabilities defined as a function of pairwise distances between the nodes in a latent space. Borrowing the conditional independence idea, we first introduce a general latent space model for brain connectomes. We assume that the number of fibers connecting brain regions are conditionally independent Poisson variables, given individual- and edge-specific rates  $\lambda_i = \{\lambda_{i1}, \dots, \lambda_{iV(V-1)/2}\}^\top$ ,

$$A_{i\ell} | \lambda_{i\ell} \sim \text{Poisson}(\lambda_{i\ell}), \quad (2.1)$$

independently for each pair  $\ell = 1, \dots, V(V-1)/2$  and  $i = 1, \dots, n$ . We assume  $\log(\lambda_{i\ell})$  has the following factorization form:

$$\log(\lambda_{i\ell}) = \gamma_\ell + \psi_\ell^{(i)}, \quad (2.2)$$

$$\psi_\ell^{(i)} = \sum_{r=1}^R \alpha_r X_{ur}^{(i)} X_{vr}^{(i)}, \quad \text{for } \ell = [uv], \quad (2.3)$$

$$\text{and } X_r^{(i)} = (X_{1r}^{(i)}, \dots, X_{Vr}^{(i)})^\top. \quad (2.4)$$

As shown in (2.2),  $\log(\lambda_{i\ell})$  is decomposed into two parts: a baseline parameter  $\gamma_\ell$  controlling connection strength between the  $\ell$ th pair of brain regions, representing shared structure across individuals, and an individual deviation  $\psi_\ell^{(i)}$ . Taking into account symmetry constraints and excluding the diagonal elements, there are  $V(V-1)/2$  unknown  $\{\lambda_{i\ell}\}$  for each subject, leading to a daunting dimensionality problem. To reduce dimensionality, [Durante et al. \(2017\)](#) proposed an SVD-type latent factorization, as shown in (2.3), where  $r = 1, \dots, R$  indexes the different latent dimensions,  $\alpha_r > 0$  is a weight on the importance of dimension  $r$ , and  $X_{ur}^{(i)}$  is the  $r$ th latent factor specific to brain region  $u$  and subject  $i$ . According to (2.3-2.4), if  $X_{ur}^{(i)}$  and  $X_{vr}^{(i)}$  have the same sign

and neither are close to zero, we have  $X_{ur}^{(i)} X_{vr}^{(i)} > 0$  and there will be a positive increment on  $\psi_\ell^{(i)}$  and hence on the expected number of fibers connecting regions  $u$  and  $v$  for subject  $i$ .

Model (2.1)-(2.4) can flexibly characterize variability across individuals in brain connectivity, while accommodating the complexity of network structures within each individual. However, we face challenges in learning the latent representations using existing latent space models: 1) Non-linearity: graph data are generally non-Euclidean with complicated structures. Designing a model to efficiently capture the non-linear structure is difficult. 2) Sparsity: brain regions are not fully connected, particularly structural brain networks. 3) speed: existing latent space approaches often rely on Markov chain Monte Carlo sampling, which is computationally intensive for high dimensional graphs. It is desirable to develop a fast non-linear factorization model. To address these challenges, we propose an autoencoder-based approach called Graph Autoencoder (GATE), from which we model the latent coordinates  $X_u^{(i)}$  of brain regions as a non-linear function of a lower-dimensional vector  $z_i$ , which serves as a low-dimensional representation of  $i$ -th brain network  $A_i$ .

### 2.2.2 The Graph AutoEncoder (GATE) Model

GATE relies on the variational autoencoder (VAE Kingma and Welling (2014)), which is a popular technique for non-linear dimension reduction. Denote  $z_i \in \mathbb{R}^K$  as a low-dimensional latent representation of the individual brain connectome  $A_i$ . GATE consists of two components. The first component is a generative model that specifies how the latent variables  $z_i$  give rise to the observations  $A_i$  through a non-linear mapping, parametrized by neural networks. The second component is an inference model that learns the inverse mapping from  $A_i$  to  $z_i$ . We frame our proposed Graph Autoencoder (GATE) method in the following context.

### 2.2.3 Generative model

For each subject  $i$ , we assume  $A_{i\ell}$  for  $\ell = 1, \dots, V(V-1)/2$  are conditionally independent given the latent representation  $z_i \in \mathbb{R}^K$ . Therefore, the likelihood of  $L(A_i)$  is

$$p_\theta(L(A_i) = a_i | z_i) = \prod_{\ell=1}^{V(V-1)/2} p_\theta(A_{i\ell} = a_{i\ell} | z_i). \quad (2.5)$$

$p_\theta(A_{i\ell} | z_i)$  is a generative model for the weighted adjacency matrix  $A_i$  given the latent  $z_i$  with  $z_i \sim p(z)$ . We define  $p(z) = N(0, I_K)$ , representing all connectomes in the same Gaussian latent space.

We learn the mapping from the Gaussian latent space to the complex observation distribution in (2.5) by a hierarchical model equipped with parameters  $\theta$ . Specifically, we assume the observations

$A_{i\ell}$  arise from the following generative process:

$$\begin{aligned} z_i &\sim N(0, I_K), \\ A_{i\ell}|z_i &\sim \text{Poisson}(\lambda_{i\ell}(z_i)), \end{aligned} \tag{2.6}$$

where the Poisson rate parameter  $\lambda_{i\ell}(z_i)$  is modeled as a nonlinear function of  $z_i$  according to:

$$\lambda_{i\ell}(z_i) = \exp(\gamma_\ell + \psi_\ell(z_i)), \tag{2.7}$$

$$\psi_\ell(z_i) = \sum_{r=1}^R \alpha_r X_{ur}(z_i) X_{vr}(z_i), \quad \text{for } \ell = [uv], \tag{2.8}$$

$$X_r(z_i) = (X_{1r}(z_i), \dots, X_{Vr}(z_i))^\top = g_r(z_i), \tag{2.9}$$

where  $g_r(\cdot) : \mathbb{R}^K \rightarrow \mathbb{R}^V$  is a nonlinear mapping from  $z_i$  to the  $r$ th latent factor of the brain regions  $X_r$ , parameterized by deep neural networks with parameters  $\theta$  for  $r = 1, \dots, R$ .

Denote  $\mathbf{X}(z_i) = (X_1(z_i), \dots, X_R(z_i)) \in \mathbb{R}^{V \times R}$ . The  $u$ -th row  $(X_{u1}(z_i), \dots, X_{uR}(z_i))$  represents the latent features of brain region  $u \in \mathcal{V}$  for individual  $i$ . A relatively large positive value for the cross product between the  $u$ -th and  $v$ -th rows implies a relatively high connection strength between these brain regions. The nonlinear mapping  $\{g_r(\cdot)\}$  ( $r = 1, \dots, R$ ) characterizes the latent embedding of brain regions that is determined via the local collaborative patterns among brain regions.

To take into account the intrinsic locality of structural brain networks, we propose a novel graph convolutional network (GCN) to learn each region’s representation by propagating node-specific  $k$ -nearest neighbor information. The intrinsic locality refers to the relative distance between brain regions measured through the length of white matter fiber tracts connecting them. We extract this information from brain imaging tractography and store it in a matrix  $B \in \mathbb{R}^{V \times V}$ , where  $B_{uv}$  is the averaged length of fiber tracts between region  $u$  and  $v$ ,  $B_{uv} = B_{vu}$ ,  $B_{uu} = 0$ , and we set  $B_{uv} = \infty$  if there are no fibers between them. For each region  $u$ , we define its  $k$ -nearest neighbors ( $k$ -NN( $u$ )) as the  $k$  ROIs closest to  $u$  according to our notion of distance, and denote the region itself as its 0-NN.

To learn the  $r$ -latent coordinate  $g_r(z_i)$  for subject  $i$ , the key idea is to consider each column  $X_r(z_i)$  as an “image” with each region as an irregular pixel; we have  $R$  such “images” for each individual. Convolutional neural networks (CNN) are highly effective architectures in image and audio recognition tasks [Krizhevsky et al. \(2012\)](#); [Sermanet et al. \(2012\)](#); [Hinton et al. \(2012\)](#), thanks to their ability to exploit the local translational invariance structures over their domain. Considering the unique features of the brain connectome networks, we generalize the CNN and define appropriate graph convolutions to learn the nonlinear mapping  $\{g_r(\cdot)\}$  via exploiting the local collaborative

pattern among brain regions. In particular, we define an  $M$ -layer GCN as follows:

$$X_r^{(i,1)} = h_1(W^{(r,1)}z_i + b_1), \quad (2.10)$$

$$X_r^{(i,m)} = h_m(W^{(r,m)}X_r^{(i,m-1)} + b_m) \quad \text{for } 2 \leq m \leq M, \quad (2.11)$$

where  $X_r^{(i,m)}$  denotes the output of the  $m$ -th layer of the convolutional neural network,  $h_m(\cdot)$  is an activation function for the  $m$ th layer, and  $W^{(r,m)}$  is a weight matrix characterizing the convolutional operator at this layer. We denote the parameters  $b_m$ ,  $W^{(r,m)}$ , together with  $\gamma_\ell$ ,  $\alpha_r$  in (2.7-2.8) ( $m = 1, \dots, M, r = 1, \dots, R, \ell = 1, \dots, V(V-1)/2$ ) as the model parameter  $\theta$ . The activation functions  $\{h_m(\cdot)\}$  can be chosen from the following candidates based on performance: (1) rectified linear unit (ReLU) function, which is widely used Goodfellow et al. (2016) in deep neural networks, with the definition as  $ReLU(x) = \max(0, x)$ , where the max operation is applied element-wise; (2) Sigmoid function defined as  $h_m(x) = \frac{1}{1+e^{-x}} \in (0, 1)$ ; (3) linear or identity function  $h_m(x) = ax$  with  $a \neq 0$ .

For  $m = 1$ ,  $W^{(r,1)} \in \mathbb{R}^{V \times K}$  maps the latent representation  $z_i \in \mathbb{R}^K$  to the latent space  $X_r^{(i,1)} \in \mathbb{R}^{V \times 1}$ ; for  $m \geq 2$ ,  $W^{(r,m)}$  is a  $V \times V$  weight matrix with the  $u$ -th row  $w_u^{(r,m)}$  satisfying  $w_{uv}^{(r,m)} > 0$  if  $v = u$  or  $v \in k_r$ -NN( $u$ ), and  $= 0$  otherwise. (2.11) implies that the embedding feature of each region at the  $m$ -th layer is determined by the weighted sum of itself and its nearest neighbor regions at the  $(m-1)$ -th layer; and the related weights aim to characterize the region-specific local connectivity. For  $r = 1, \dots, R$ , we can choose different values of  $k$  to define its  $k_u$ -NN to fully explore the possible collaboration pattern among brain regions.

Figure 2 shows how a three-layer GCN learns  $X_r(z_i)$  via a 2-NN GCN. First, we initialize the latent feature for each region as  $x_{ur}^{(i,1)}$  based on (2.10). Then, we construct a ‘‘graph’’ based on the fiber length in  $B$ : each region is assigned to connect with 2 nearest neighbors at most according to the fiber length to other brain regions. If a region  $u$  has less than  $k = 2$  direct neighbors, we will include all the regions  $v$  satisfying  $B_{uv} \in (0, \infty)$  as its neighbors. This information is reflected in  $W^{(i,m)}$ , whose rows contain at most three non-zero elements (one at the diagonal and two off the diagonal). Next, we update the latent feature of each region in the next layer based on a sum of reweighted features from its 2 nearest neighbors and itself.

We collect all the parameters  $(\gamma_\ell, \alpha_r, b_m, W^{(r,m)})$  for  $\ell = 1, \dots, V(V-1)/2, r = 1, \dots, R, m = 1, \dots, M$  as  $\theta$ . In the following Section 2.2.4, we show how to use variational inference to learn  $\theta$ .

### 2.2.4 Variational Inference and GATE Learning

To train and evaluate the deep generative model in (2.6), we need to estimate  $\theta$ , the parameters characterizing the mapping from  $z_i$  to  $A_{il}$  and  $p_\theta(z_i|A_i)$ , the posterior distribution of the latent

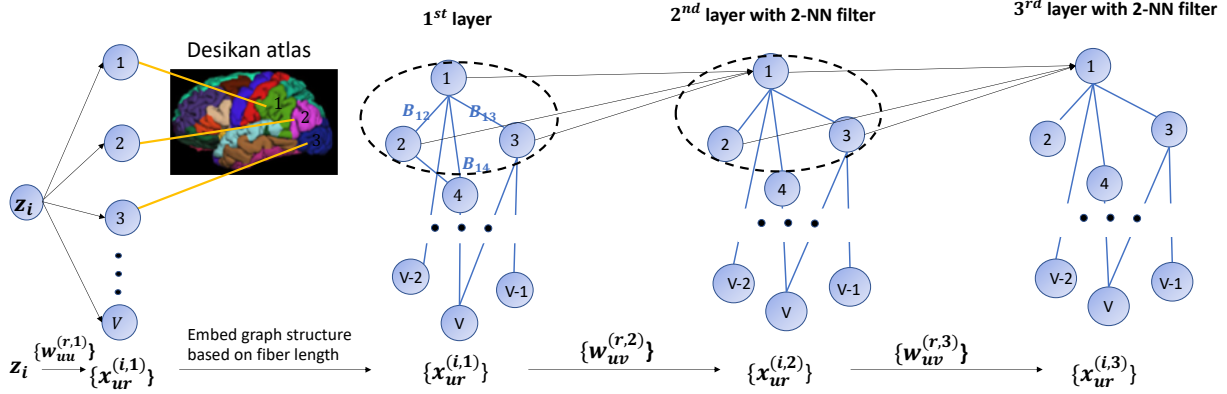


Figure 2: Illustrative example of three-layer GCN architecture with 2-NN filters. For example, for node 1, the 2-NN is node 2 and node 3.  $x_{1r}^{(i,1)} = h_1(w_{11}^{(r,1)} z_i)$ ,  $x_{1r}^{(i,2)} = h_2(w_{11}^{(r,2)} x_{1r}^{(i,1)} + w_{12}^{(r,2)} x_{2r}^{(i,1)} + w_{13}^{(r,2)} x_{3r}^{(i,1)})$ .

variable. By applying Bayes' rule, we have the posterior as

$$p_\theta(z_i|A_i) = \frac{p_\theta(A_i|z_i)p(z_i)}{p_\theta(A_i)}.$$

Since the likelihood function  $p_\theta(A_i|z_i)$  is parameterized via the neural network with non-linear transformations, both the marginal distribution  $p_\theta(A_i)$  and the posterior probability distribution  $p_\theta(z_i|A_i)$  are intractable. Hence, we resort to variational inference (VI) (Jordan et al. (1999), Hoffman et al. (2013)), a widely-used tool for approximating intractable posterior distributions. VI seeks a simple distribution  $q_\phi(z_i|A_i)$  parameterized by  $\phi$  from a variational family, e.g., a Gaussian distribution family, that best approximates  $p_\theta(z_i|A_i)$ . We call such  $q_\phi(z_i|A_i)$  as the probabilistic encoder, which maps the input  $A_i$  to a low dimensional latent representation  $z_i$ . The approximated posterior  $q_\phi(z_i|A_i)$  should be close to  $p_\theta(z_i|A_i)$ . We use Kullback-Leibler (KL) divergence to quantify the separation between these two distributions, which is defined as  $D_{KL}(Q||P) = \mathbb{E}_{z \sim Q} \log \frac{Q(z)}{P(z)}$ , measuring how much information is lost if the distribution  $Q$  is used to represent  $P$ . We choose

$$q_\phi(z_i|A_i) \sim N(\mu_\phi(A_i), \text{diag}\{\sigma_\phi^2(A_i)\}), \quad (2.12)$$

i.e., a fully factorized (diagonal covariance) Gaussian distribution, to facilitate computation. We design deep neural networks to learn the parameters in  $\mu_\phi$  and  $\sigma_\phi^2$ , and denote the parameters involved in deep neural networks as  $\phi$ . The details are in Supplementary S.1.

Our objective is to maximize the observed data log-likelihood  $\log p_\theta(A_i)$ , and also minimize the difference between the true posterior  $p_\theta(z_i|A_i)$  and approximated posterior distribution  $q_\phi(z_i|A_i)$ .

We express the above objective as

$$\begin{aligned} & \log p_\theta(A_i) - D_{KL}(q_\phi(z_i|A_i)||p_\theta(z_i|A_i)) \\ &= \mathbb{E}_{q_\phi(z_i|A_i)}[\log p_\theta(A_i|z_i)] - D_{KL}(q_\phi(z_i|A_i)||p_\theta(z_i)) := -\mathcal{L}(A_i; \theta, \phi), \end{aligned} \quad (2.13)$$

where detailed calculation of (2.13) can be found in Supplementary S.2. Since  $D_{KL}(q_\phi(z_i|A_i)||p_\theta(z_i|A_i))$  is nonnegative,  $-\mathcal{L}(A_i; \theta, \phi)$  can be viewed as a lower bound on the marginal log-likelihood, referred to as the evidence lower bound (ELBO), which is a function of both  $\theta$  and  $\phi$ . Therefore, the training objective is minimizing the negative of the ELBO, i.e., minimizing

$$\mathcal{L}(A_i; \theta, \phi) = -\mathbb{E}_{q_\phi(z_i|A_i)}[\log p_\theta(A_i|z_i)] + D_{KL}(q_\phi(z_i|A_i)||p(z_i)). \quad (2.14)$$

$\mathcal{L}(A_i; \theta, \phi)$  consists of two parts: the first term is the reconstruction error, measuring how well the model can reconstruct  $A_i$ ; while the second term, defined as the KL divergence of the approximate posterior from the prior, is a regularizer that pushes  $q_\phi(z_i|A_i)$  to be as close as possible to its prior  $N(0, I_K)$ .

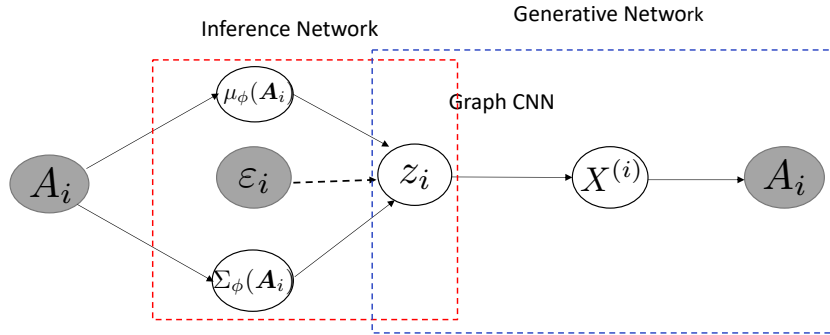


Figure 3: A taxonomy of GATE. Dashed lines with arrow denote sampling operations.

In practice, the expectation in the ELBO (2.14) is intractable. To address this, we employ Monte Carlo variational inference Kingma and Welling (2014) by approximating the troublesome expectation with samples of the latent variables from the variational distribution  $z_i \sim q_\phi(z_i|A_i)$ . Particularly, we form the Monte Carlo estimates of the expectation as

$$\mathbb{E}_{q_\phi(z_i|A_i)}[\log p_\theta(A_i|z_i)] \simeq \frac{1}{L} \sum_{\ell=1}^L \log p_\theta(A_i|z_i^\ell),$$

where  $z_i^\ell$  is sampled with the reparametrization trick: sampling  $\varepsilon_i^\ell \sim N(0, I_K)$  and reparametrizing  $z_i^\ell = \mu_\phi(A_i) + \varepsilon_i^\ell \odot \Sigma_\phi(A_i)$ , where  $\Sigma_\phi(A_i) = \text{diag}\{\sigma_\phi^2(A_i)\}$ . Simple calculation shows that the KL-divergence  $D_{KL}(q_\phi(z_i|A_i)||p(z_i)) = \frac{1}{2} \sum_{k=1}^K (\mu_k^2 + \sigma_k^2 - 1 - \log(\sigma_k^2))$ , where  $\mu_k$  and  $\sigma_k$  are the

$k$ -th element of  $\mu_\phi(A_i)$  and  $\Sigma_\phi(A_i)$  respectively. Therefore, the ELBO in (2.14) can be approximated as

$$\mathcal{L}(A_i; \theta, \phi) \simeq \tilde{\mathcal{L}}(A_i; \theta, \phi) = -\frac{1}{L} \sum_{\ell=1}^L \log p_\theta(A_i | z_i^\ell) + \frac{1}{2} \sum_{k=1}^K (\mu_k^2 + \sigma_k^2 - 1 - \log(\sigma_k^2)),$$

which is differentiable with respect to  $\theta$  and  $\phi$ . Then, given  $n$  observed networks, we can construct an estimator of the ELBO of the full dataset, based on the minibatches  $\frac{n}{m} \sum_{i=1}^m \tilde{\mathcal{L}}(A_{(i)}; \theta, \phi)$ , where  $\{A_{(i)}\}_{i=1}^m$  is a randomly drawn sample of size  $m$  from the full observed data with sample size  $n$ . Viewing  $\frac{n}{m} \sum_{i=1}^m \tilde{\mathcal{L}}(A_{(i)}; \theta, \phi)$  as the objective, we implement a stochastic variational Bayesian algorithm to optimize  $\theta$  and  $\phi$ , respectively. Figure 3 shows the graphical diagram of the GATE approach; Algorithm 1 summarizes the GATE training procedure.

---



---

**Input:**  $\{A_i\}_{i=1}^n$ ,  $\{z_i\}_{i=1}^n$ , geometric matrix  $B$ , latent space dimension  $R$ .

---

Randomly initialize  $\theta, \phi$

**while** not converged **do**

Sample a batch of  $\{A_i\}$  with mini-batch size  $m$ , denote as  $\mathcal{A}_m$ .

**for all**  $A_i \in \mathcal{A}_m$  **do**

Sample  $\varepsilon_i \sim N(0, I_R)$ , and compute  $z_i = \mu_\phi(A_i) + \varepsilon_i \odot \Sigma_\phi(A_i)$ .

Compute the gradients  $\nabla_\theta \tilde{\mathcal{L}}(A_i; \theta, \phi)$  and  $\nabla_\phi \tilde{\mathcal{L}}(A_i; \theta, \phi)$  with  $z_i$ .

Average the gradients across the batch.

Update  $\theta, \phi$  using gradients of  $\theta, \phi$ .

**Return**  $\theta, \phi$ .

---



---

Table 1: Algorithm 1: Training GATE model using gradients.

### 2.3 Regression with GATE and Inference

**Relating brain connectomes with traits.** In addition to finding low-dimensional representations of brain structure networks, we are also interested in inferring the relationship between brain networks and human traits, such as cognition. With this goal in mind, we develop a supervised version of GATE referred to as regression GATE (reGATE). Let  $y_i$  be a trait of the  $i$ -th subject. We first express the joint log likelihood of  $(A_i, y_i)$  as

$$\log p_\theta(A_i, y_i) = -\mathcal{L}(A_i, y_i; \theta, \phi) + D_{KL}(q_\phi(z_i | A_i) || p_\theta(z_i | y_i, A_i)), \quad (2.15)$$

where

$$-\mathcal{L}(A_i, y_i; \theta, \phi) = \mathbb{E}_{q_\phi(z_i | A_i)} \log p_\theta(y_i | z_i) + \mathbb{E}_{q_\phi(z_i | A_i)} \log p_\theta(A_i | z_i) - D_{KL}(q_\phi(z_i | A_i) || p_\theta(z_i))$$

is called the ELBO of  $\log p_\theta(A_i, y_i)$ ; we show the derivation of (2.15) in Supplementary S.3. In (2.15), we divide the log-likelihood of  $(A_i, y_i)$  into two parts: the ELBO denoted as  $-\mathcal{L}(A_i, y_i; \theta, \phi)$ , and the non-negative KL-divergence between  $q_\phi(z_i|A_i)$  and  $p_\theta(z_i|y_i, A_i)$ . Different from the unsupervised ELBO in (2.13), (2.15) can be considered as a supervised ELBO with an extra term  $p_\theta(y_i|z_i)$  that essentially formulates a regression of  $y_i$  with respect to  $z_i$ . Here we consider  $y_i$  as a continuous random variable, and set  $p_\theta(y_i|z_i)$  as a univariate Gaussian, i.e.,  $p_\theta(y_i|z_i) \sim N(z_i^\top \beta + b, \sigma^2)$ , where  $\beta, \sigma^2 \in \theta$  are parameters to be learned. Figure 4 shows the flowchart of the reGATE architecture.

Similarly to Section 2.2.4, we form the Monte Carlo estimate of  $\mathcal{L}(A_i, y_i; \theta, \phi)$  and estimate  $\theta, \phi, \beta, b$  following the stochastic variational Bayesian Algorithm 1 by replacing  $\mathcal{L}(A_i; \theta, \phi)$  with  $\mathcal{L}(A_i, y_i; \theta, \phi)$ . We show the detailed sampling steps in Supplementary S.4.

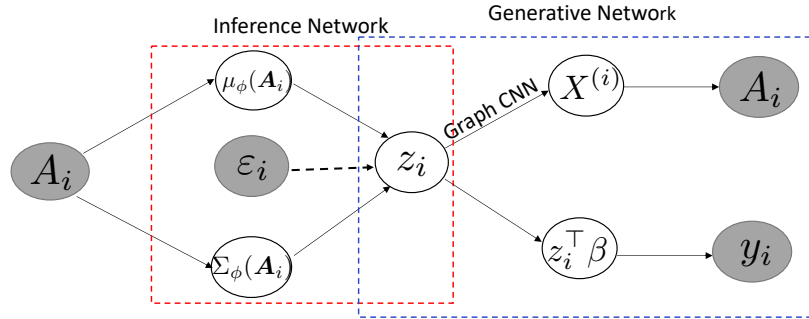


Figure 4: reGATE to predict human traits. Dashed lines with an arrow denote sampling operations.

**Conditional generative model:** We are interested in inferring how brain networks vary across levels of a trait. For example, if  $y_i$  measures a person’s memory ability, we would like to study differences in the distribution of brain networks between people with good and bad memory skills. To address questions of this type, we generate samples from the posterior distribution of  $A_i$  given particular  $y_i$  values using Gibbs sampling: sample  $z_i$  from  $p_\theta(z_i|y_i)$ , then sample  $A_i$  from  $p_\theta(A_i|z_i)$ . The conditional  $p_\theta(A_i|z_i)$  is learned while implementing reGATE. The posterior distribution of  $z_i$  given  $y_i$  can be expressed as  $p_\theta(z_i|y_i) \propto p_\theta(y_i|z_i)p_\theta(z_i)$ , where  $p_\theta(z_i) \sim N(0, I_K)$  and  $p_\theta(y_i|z_i) \sim N(z_i^\top \beta + b, \sigma^2)$ . Therefore, we have  $p_\theta(z_i|y_i) \sim N(\mu_z(y_i), \Sigma_z(y_i))$ , where

$$\mu_z(y_i) = (I_K + \beta\beta^\top/\sigma^2)^{-1}\beta(y_i - b)/\sigma^2, \quad \text{and} \quad \Sigma_z(y_i) = (I_K + \beta\beta^\top/\sigma^2)^{-1}; \quad (2.16)$$

the derivation of (2.16) is in Supplementary S.5.

The latent representation  $z_i$  is unidentifiable in VAE since the log-likelihood and ELBO are rotationally invariant for  $z_i$ . For example, letting  $\tilde{z}_i = U^\top z_i$ , then  $P_{U,\theta}(A_i) = P_\theta(A_i)$  and

$$D_{KL}(q_{U,\phi}(z_i|A_i)||p_{U,\theta}(z_i|A_i)) = D_{KL}(q_\phi(z_i|A_i)||p_\theta(z_i|A_i)),$$

where  $U$  is an orthogonal matrix,  $q_{U,\phi}(\cdot)$  and  $p_{U,\theta}(\cdot)$  are defined by replacing  $z_i$  with  $\tilde{z}_i$  in  $q_\phi(\cdot)$  and  $p_\theta(\cdot)$ . Rotational invariance can be solved by post-processing to rotationally align the  $z_i$ 's. However, this would only be necessary if one is attempting to compare  $z_i$ s from different datasets or analyses of a given dataset. Within an analysis, the main focus is on inference on the relative values of  $z_i$ s, and these relative values are well defined. In addition, when the focus is on relating brain structure to human traits or in predicting traits based on brain structure or vice versa, the non-identifiability issue does not present a problem.

### 3 Simulation Study

We conduct a simulation study to evaluate the performance of GATE and reGATE in accurately characterizing brain networks and predicting human traits. We simulate from four network structures: sparse networks according to the model in [Johnson \(1977\)](#), community structures under the model of [Nowicki and Snijders \(2001\)](#), small-worldness from the model in [Watts and Strogatz \(1998\)](#), and scale-free property from the model in [Barabási and Albert \(1999\)](#). We simulate 100 networks with  $V = 68$  nodes for each type by sampling their edges from conditional independent Bernoulli random variables given their corresponding structure-specific edge probability. Each structure-specific edge probability vector is carefully constructed to assign high probability to a subset of network configurations characterized by a specific property. [Figure 5](#) displays some example networks we generated with the four different network structures.

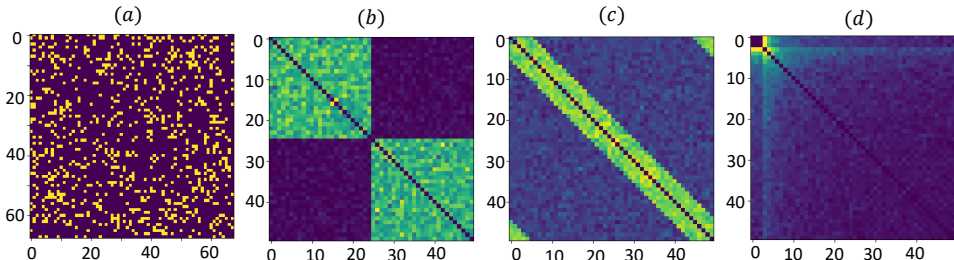


Figure 5: The edge probability vectors (rearranged in matrix form) from four network structures: (a) sparse graph, (b) community structure, (c) small world, (d) scale free.

We first generate  $y_i$  according to  $y_i = \alpha^\top A_i \alpha + \epsilon_i$ , where  $\alpha = (\underbrace{1, \dots, 1}_{17}, 0, \dots, 0)^\top \in \mathbb{R}^{68}$ , and  $\epsilon_i \sim N(0, 1)$ . We then standardize  $y_i$ , so that it ranges from  $-1.5$  to  $2.0$ . These settings aim to generate separable  $y_i$ 's according to the topological structures of  $A_i$ . The histograms in [Figure 7](#) clearly demonstrate how  $y_i$  varies for different network structures. Our goals in this simulation study include (1) learning the latent representation under both GATE and reGATE; (2) inferring

how the network connectivity structure varies with  $y_i$ ; (3) assessing the predictive performance of the reGATE model.

We train GATE and reGATE to obtain low-dimensional representations  $z_i$ 's. We then conduct PCA analysis on the posterior mean of  $z_i|A_i$  and plot the first two PC scores in  $\mathbb{R}^2$  colored according to the corresponding  $y$  value. We can clearly observe the separation between these four types of networks in the low-dimensional representation space inferred using both GATE and reGATE, with reGATE yielding greater separation across the groups.

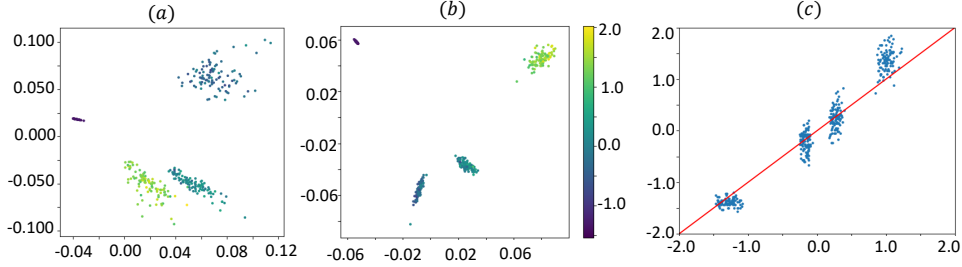


Figure 6: Plot of the first 2 PC scores of the posterior mean of  $z_i|A_i$  with corresponding  $y_i$ . Different colors refer to various values of  $y$ . (a) GATE, (b) reGATE. (c) Predicted  $y$  v.s. true  $y$  in reGATE, where x-axis is the true value and y-axis is the predicted value.

To infer how brain networks  $A_i$  vary according to  $y_i$ , we simulate networks from the posterior distribution of  $A_i|y_i$  according to the conditional generative model in Section 2.3. Specifically, we first sample  $z_i | y_i$  based on equation (2.16) with the parameters obtained from the previously trained reGATE and  $y_i$  ranging from  $-1.5$  to  $2$ , then generate networks via  $p_\theta(A_i | z_i)$ . Figure 7 shows the generated networks with structure varying for different  $y_i$ s. We can clearly observe that the network shows a sparse structure when  $y_i = -1.5$ , a mixture of community and small-world structure when  $y_i = -0.1$ , and a clear scale free structure when  $y_i = 2$ . These generated structures are consistent with the ground truth in our simulation settings.

To address our third goal, we evaluate the predictive accuracy of reGATE. We consider two cases: (1)  $y_i = \alpha^\top A_i \alpha + \epsilon_i$ ; (2)  $y_i = (\alpha^\top A_i \alpha)^2 + (\alpha^\top A_i \alpha)^3 + \epsilon_i$ . We also compare reGATE with a few popular methods in the literature for predicting human traits using network data. The first method is a regular linear regression based on tensor network principal component analysis (LR-TNPCA) in Zhang et al. (2019). The second method is linear regression based on a regular PCA applied to the vectorized networks. The third method is tensor regression proposed in Zhou et al. (2013), denoted as CPR here. The mean square error (MSE) from five-fold cross validation was used to compare different approaches. Figure 6 (c) shows the association between the predicted value and the true value under reGATE in case 1. The first and second row in Table 2 show the MSE under different methods. We can see reGATE outperforms other methods in predictive accuracy. The third row

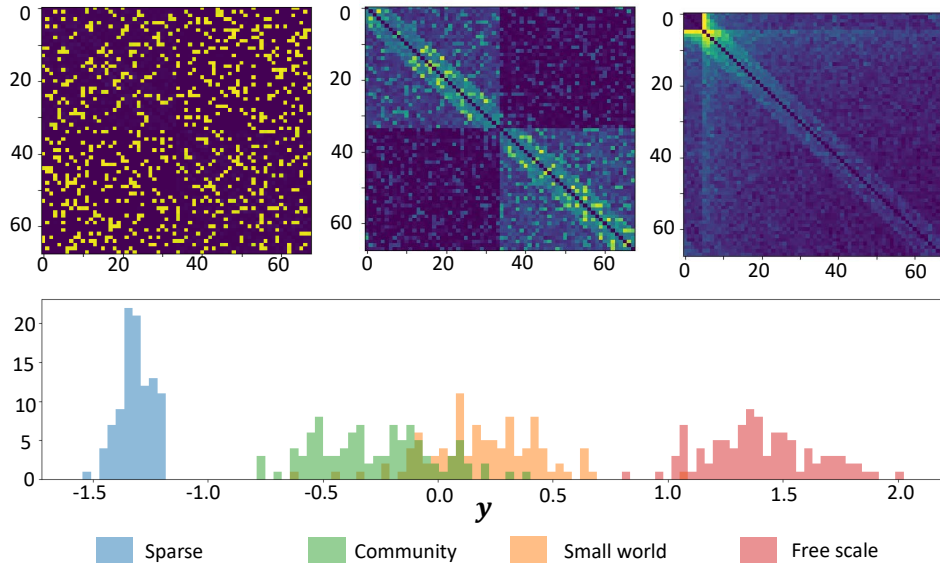


Figure 7: First row: generated networks conditional on the specific  $y_i$  using reGATE, corresponding to  $y_i = -1.5, -0.1, 2$  respectively from left to right. Second row: histogram of  $y_i$  with respect to the network structure; x-axis is the value of  $y_i$ , y-axis is the frequency that belongs to a specific structure in the training data.

in Table 2 reports the computing time with 100 replicated simulations. reGATE is both fast and accurate based on these results.

	reGATE	LR-TNPCA	LR-PCA	CPR
MSE: case 1	<b>0.0252</b>	0.0271	0.0340	0.0388
MSE: case 2	<b>0.0505</b>	0.0593	0.0700	0.1078
Time (mins)	17.5	197.6	5.3	253.7

Table 2: The first row and the second row are the MSE under different methods. All numbers are calculated based on the mean of 100 replicated simulations.

We summarize the computing details used in the simulation study here. We run stochastic gradient descent with momentum (the Adam algorithm in Kingma and Ba (2015)) on GATE and reGATE with learning rate 0.001 on 2 NVIDIA Titan-V GPUs. In GATE, we use a batch size of 128, sampled uniformly at random at each epoch and repeated for 1000 epochs. In reGATE, we use 5-fold CV to calculate the MSE, and run 200 epochs with batch size of 128 for each training dataset. The experimental details and network architectures for the inference model and generative model training are summarized in Table 3. The latent dimension  $K$  is chosen as the smallest value that achieves the minimal training loss, provided that the network architectures are fixed as in Table 3.

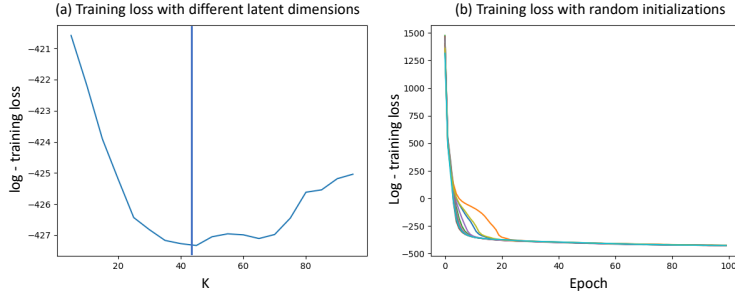


Figure 8: (a) log-training loss with latent dimension  $K$  varies; (b) the paths of the log-training loss with random initializations.

Figure 8 (a) shows the log-training loss with latent dimensions  $K$  varying from 5 to 100, and the training loss achieves the best performance when  $K$  is around 45. The sensitivity of the training loss with respect to the random initialization is also explored. As shown in Figure 8 (b), under different initializations, the paths of the training loss converge to the same level as the number of epochs increases. All code used to produce the results and figures is available online via GitHub (<https://github.com/meimeiliu/GATE>).

	Inference model ( $\mu_\phi, \sigma_\phi$ )		Generative model	
	$\mu_\phi$ ( $N = 2$ )	$\sigma_\phi$ ( $N = 2$ )	setting	activation
GATE/reGATE ( $K = 45$ )	$W_{1,\mu} : 45 * 400$ $W_{2,\mu} : 400 * 45$ $b_{1,\mu} : 400 * 1$ $b_{2,\mu} : 45 * 1$ $\varphi_{1,\mu} = \text{ReLu}$ $\varphi_{2,\mu} = \text{Linear}$	$W_{1,\sigma} : 45 * 400$ $W_{2,\sigma} : 400 * 45$ $b_{1,\sigma} : 400 * 1$ $b_{2,\sigma} : 45 * 1$ $\varphi_{1,\sigma} = \text{Relu}$ $\varphi_{2,\sigma} = \text{Linear}$	$k\text{-NN}: 16$ $M = 2$ $R = 5$	$h_1: \text{Sigmoid}$ $h_2: \text{Sigmoid}$

Table 3: Experimental details and network architectures.  $K$  is the dimension of  $z_i$ ,  $N$  is the number of layers in the inference network,  $M$  is the number of layers in GCN, and  $R$  is the dimension of  $X^{(i)}$ .

## 4 Applications to the ABCD and HCP data

We apply our method to both the ABCD and HCP datasets described in Section 2.1 to examine the relationship between structural brain networks and cognition for adolescents and young adults. The ABCD study uses a reliable and well-validated battery of measures that assess a wide range of human functions, including cognition. The core of this battery is comprised of the tools and methods developed by the NIH Toolbox for assessment of neurological and behavioral function Gershon et al.

(2013). The Toolbox includes measures of cognitive, emotional, motor and sensory processes. Since we are particularly interested in cognition, we extract four cognition related measures as  $y$  from ABCD, including

- (a) Picture vocabulary test: the picture vocabulary test uses an audio recording of words, presented with four photographic images on the computer screen. Participants are asked to select the picture that best matches the meaning of the word.
- (b) Oral reading recognition test: participants on this test are asked to read and pronounce letters and words as accurately as possible.
- (c) Crystallized composite score: crystallized cognition composite can be interpreted as a global assessment of verbal reasoning. We use the age-corrected standard score.
- (d) The cognition total composite score: this composite score measures overall cognition and is obtained from a factor analysis Heaton et al. (2014).

We extracted two matched cognitive measures from HCP: picture vocabulary test score and oral reading recognition test. In addition, we add two more cognitive measures in our data analysis: total number correct answers and total positions off in a line orientation test. More detailed description of these traits can be found in Gershon et al. (2013).

#### 4.1 Visualization: show network data in low-dimensional space

Both GATE and reGATE output low-dimensional representations of the brain networks. We can visualize the latent features of each individual’s connectome, and examine the relationship between structural connectivity and the four traits via the latent features. We train GATE on 5252 brain networks extracted from the ABCD dataset to obtain low-dimensional representations  $z_i$  for  $i = 1, \dots, 5252$ . We then plot the posterior mean of  $z_i | A_i$  using t-SNE Van der Maaten and Hinton (2008) colored with its corresponding trait score in  $\mathbb{R}^3$ . For each cognition trait, we show 200 subjects’ data, with the first 100 subjects having the lowest trait scores and the second 100 subjects having the highest scores. As shown in Figure 9 (a) – (d), under both GATE and reGATE, we obtain large separation between the two groups of subjects, indicating that brain connection patterns are different for these groups. ReGATE has better performance since we incorporate the trait information in learning the  $z_i$ s. A similar analysis is conducted using the HCP data, and the result is shown in Figure 15 in the supplement.

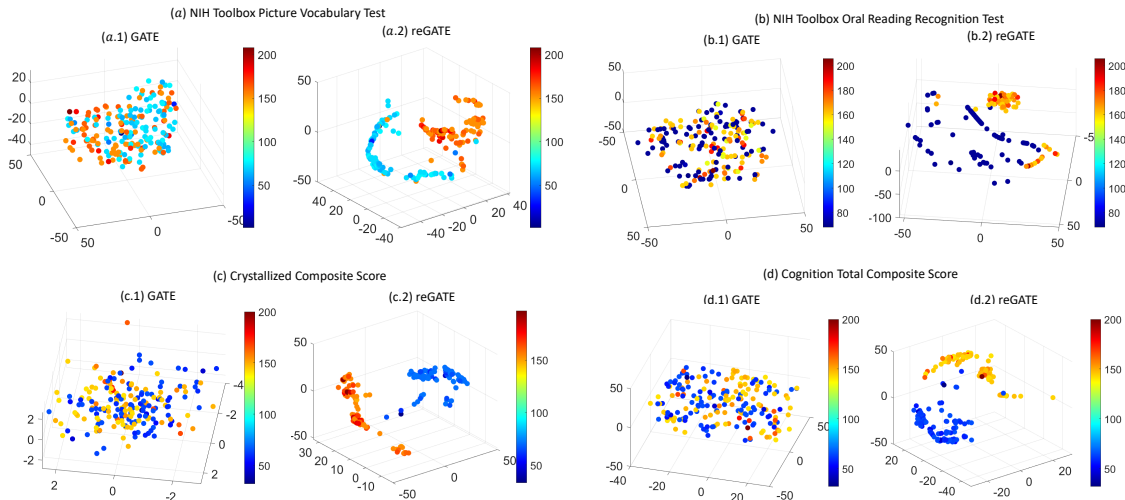


Figure 9: Visualization of low dimensional embedding  $z_i$  learned from GATE and reGATE applied to the ABCD study. For each trait, we display 100 subjects with the lowest trait scores and 100 subjects with the highest scores. Colors represent the trait scores.

## 4.2 Prediction: predict traits with reGATE

In this section, we demonstrate the predictive ability of reGATE, and compare it with several competitors: LR-TNPCA [Zhang et al. \(2019\)](#), LR-PCA, CPR [Zhou et al. \(2013\)](#), and BLR [Wang et al. \(2019\)](#). BLR is supervised bi-linear regression (BLR) with emphasis on signal sub-network selection. The MSE from five-fold cross validation is used to assess performance. Table 4 shows results for the ABCD and HCP datasets. reGATE significantly outperforms other methods in both datasets for all studied traits. With the bigger sample size ( $n = 5252$ ) in the ABCD data, the improvements of reGATE are much higher compared to those for the HCP data. It is well known that deep neural networks tend to perform particularly well for large training sample sizes.

We also calculate the percentage of MSE improvement upon a baseline model, the sample mean  $\bar{y}$ , for the prediction result from the ABCD data. As shown in Figure 10, most methods demonstrate an improved MSE compared with the sample mean  $\bar{y}$ , indicating that there is a detectable relationship between the structural connectome and cognitive traits. However, reGATE achieves stable and significant prediction improvements ranging from 30% to 40%, while the competitors' performance improvements fluctuate from  $-5\%$  to  $5\%$ .

Besides MSE, we evaluate the correlation between the predicted value  $\hat{y}_i$  and the observed value  $y_i$  via five-fold cross validation for different approaches. Correlation is reported in the parenthesis in Table 4. We can see that reGATE significantly improves the prediction by increasing the correlation from around 0.2 to 0.4.

	reGATE	LR-TNPCA	LR-PCA	CPR	BLR
ABCD ( $n = 5252$ )					
Pic Voc	<b>186.8 (0.40)</b>	280.1 (0.22)	285.2 (0.20)	285.1 (0.23)	200.4 (0.29)
Oral Reading	<b>206.5 (0.41)</b>	342.3 (0.19)	346.5 (0.14)	357.0 (0.13)	337.1 (0.19)
Cryst Comp	<b>279.4 (0.39)</b>	315.8 (0.23)	322.9 (0.22)	318.4 (0.19)	321.3 (0.30)
CogTot Comp	<b>248.0 (0.38)</b>	297.6 (0.17)	308.6 (0.26)	306.7 (0.22)	290.2 (0.32)
HCP ( $n = 1065$ )					
Pic Voc	<b>209.1 (0.28)</b>	214.5 (0.25)	219.0 (0.21)	257.2 (0.17)	216.1 (0.23)
Oral Reading	<b>198.9 (0.26)</b>	202.1 (0.22)	204.2 (0.21)	252.1 (0.19)	200.4 (0.26)
LO: correct number	<b>17.8 (0.27)</b>	18.5 (0.23)	18.2 (0.22)	21.9 (0.19)	18.8 (0.18)
LO: positions off	<b>195.8 (0.27)</b>	201.8 (0.22)	202.6 (0.24)	259.0 (0.19)	200.7 (0.27)

Table 4: Comparison of prediction results of different methods in both the ABCD and HCP datasets. Each cell shows the MSE and correlation (in the parenthesis) between the observed and predicted measures via five-fold CV.

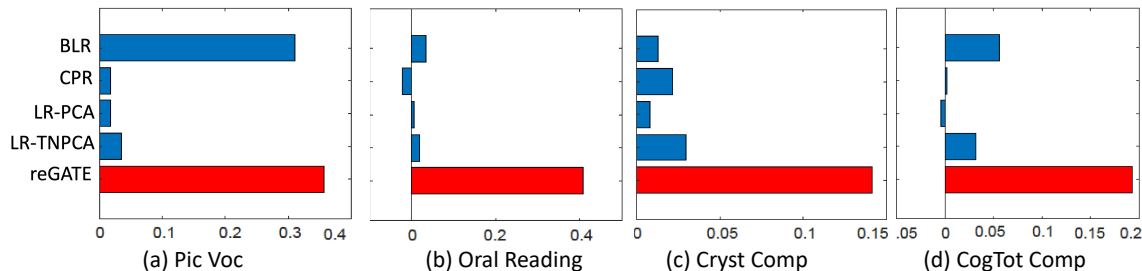


Figure 10: Percentage of the MSE improvement compared with a baseline method of using  $\bar{y}$  as the predicted trait. (a) Picture vocabulary score, (b) oral reading recognition test score, (c) crystallized composite age-corrected standard score, and (d) cognition total composite score. X-axis is the improved proportion; y-axis marks different methods. The analysis is conducted using the ABCD data.

### 4.3 Inference: generate brain connectomes conditioned on traits

An appealing characteristic of reGATE is the ability to generate brain networks for new individuals conditionally on their trait value. This facilitates inference on how brain networks, and their topological properties, change across different levels of a trait and how this dependence varies across individuals. In our first experiment, we assess the performance of GATE in characterizing the observed brain network data via posterior predictive checks [Gelman et al. \(2013\)](#) for relevant network topological properties, including network density, mean eigencentality, and average path length. Denote  $\eta_k = g_k\{L(\mathcal{A})\}$  as the random variable associated with the  $k$ th network summary

measure, for  $k = 1, 2, 3$ , where  $\mathcal{A}$  represents the brain connectomes. Then we calculate the posterior predictive distributions for these summary measures based on the generative model  $p_\theta(\mathcal{A} | z)$  in Section 2.2.3 as  $p_{\eta_k}(\eta | z) = \sum_{a \in \mathbb{A}_v: g_k(a) = \eta} p_\theta(\mathcal{A} = a | z)$ , for  $k = 1, 2, 3$ , respectively. Figure 11 compares the network summary measures computed using all 1065 subjects from the HCP data (white-colored) and the generated network data (gray-colored) from GATE. GATE achieves good performance in characterizing the observed network summary measures.

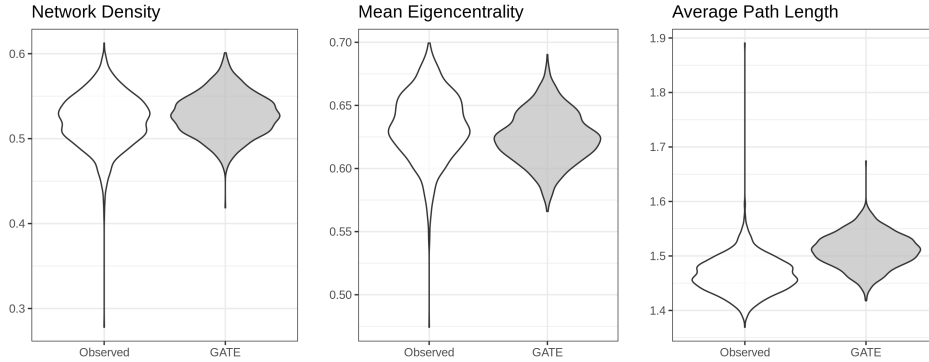


Figure 11: HCP: Goodness-of-fit assessments for selected network summary measures. The violin plots summarize the distribution in the observed data (white), and the posterior predictive distribution arising from GATE (gray).

We next consider the conditional predictive distribution of network topological summaries given trait scores, i.e.,  $\eta_k | y$ . We consider network density and average path length for both the ABCD and HCP data, and focus on different levels of picture vocabulary test score as  $y$ . The distribution of  $\eta_k | y$  can be expressed as  $p_{\eta_k}(\eta | y) = \sum_{a \in \mathbb{A}_v: g_k(a) = \eta} p_\theta(\mathcal{A} = a | y)$ , for  $k = 1, 2$ , respectively, where  $p_\theta(\mathcal{A} = a | y)$  can be obtained via the conditional generative model in Section 2.3. As shown in Figure 12, the network density increases and the average path length decreases as the picture vocabulary score increases. There is more variability in network topological summaries for the adolescent subjects in ABCD than for the adults in HCP.

We next explore how the brain network varies across different levels of trait  $y$ . For each trait, we consider three levels that range from the minimum to the maximum, and generate multiple networks for each trait value. For example, for the oral reading recognition score in the HCP, we consider  $y = 60, 91$  and  $138$ , and generate brain networks according to the conditional generative procedure in Section 2.3. A mean network is used to summarize the generated network data for a given  $y$ , and we further dichotomize the connectome to  $\{0, 1\}$  depending on whether a connection exists for better visualization. The results are shown in Figure 13, where the first column shows histograms of the observed trait scores, and the second to the fourth columns show the generated

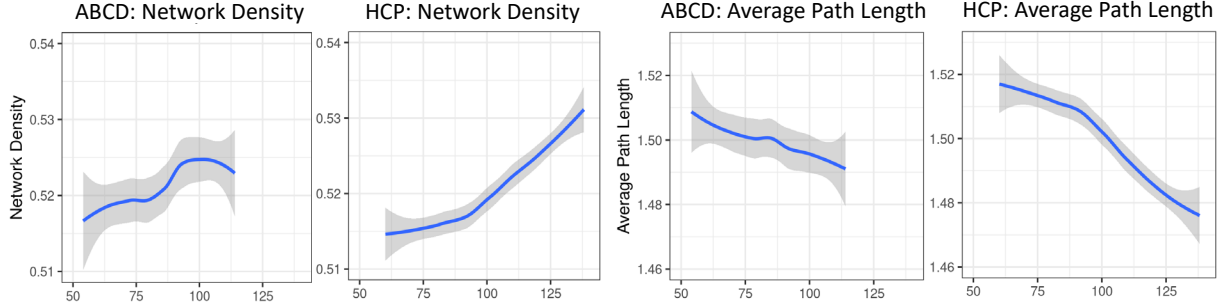


Figure 12: ABCD and HCP: posterior predictive network summaries with confidence bands for network density and average path length. X-axis is the picture vocabulary test score. The confidence bands are calculated based on 500 generated network summaries conditional on different picture vocabulary test scores.

mean networks (with the first 34 nodes from the left side of the brain and the next 34 nodes from the right side of the brain; The Supplement contains a table with descriptions of each ROI) for different  $y$ . From the result in the first row, more connections between the two hemispheres of the brain is correlated with better reading ability. In the second row, we observe the same pattern for the line orientation trait. This result is consistent with findings in the literature [Bullmore and Sporns \(2009\)](#); [Durante and Dunson \(2018\)](#).

To enhance the above analysis, we reduce the number of levels and select only the 10%th and 90%th quantiles from the observed  $y$  as two representative levels. For each level, we generate 100 conditional networks  $A_i | y_i$  and calculate the mean difference between the networks in the high and low trait groups. Figure 14 plots the top 50 connections (based on absolute values) in the mean difference network for the picture vocabulary test for both HCP and ABCD. This procedure is done separately for the two datasets. The 50 connections are further separated into positive and negative connections and are plotted in separate panels in Figure 14. After ranking the connections by absolute values, these connections are dominated by positive ones, indicating that better vocabulary ability is associated with more connections.

The first row in Figure 14 shows results from the HCP data, and the second row shows results from the ABCD data. Considering the different populations (young adults vs adolescents) in our data analysis, it is interesting to observe many similar results. For example, we observe denser connections both within the left and right frontal lobes and between them. In particular, we see that brain regions such as  $l26, r26$  (rostral middle frontal),  $l27, r27$  (superior frontal), and  $l3, r3$  (caudal middle frontal) are densely involved (nodes with high degrees) in the top 50 connections. These brain regions are thought to contribute to higher cognition and particularly working memory [Boisgueheneuc et al. \(2006\)](#), and are important for language-related activities [Binder et al. \(1997\)](#); [Friederici \(2002\)](#). We also observe that the four nodes in the occipital lobe (regions 4, 10, 12 and

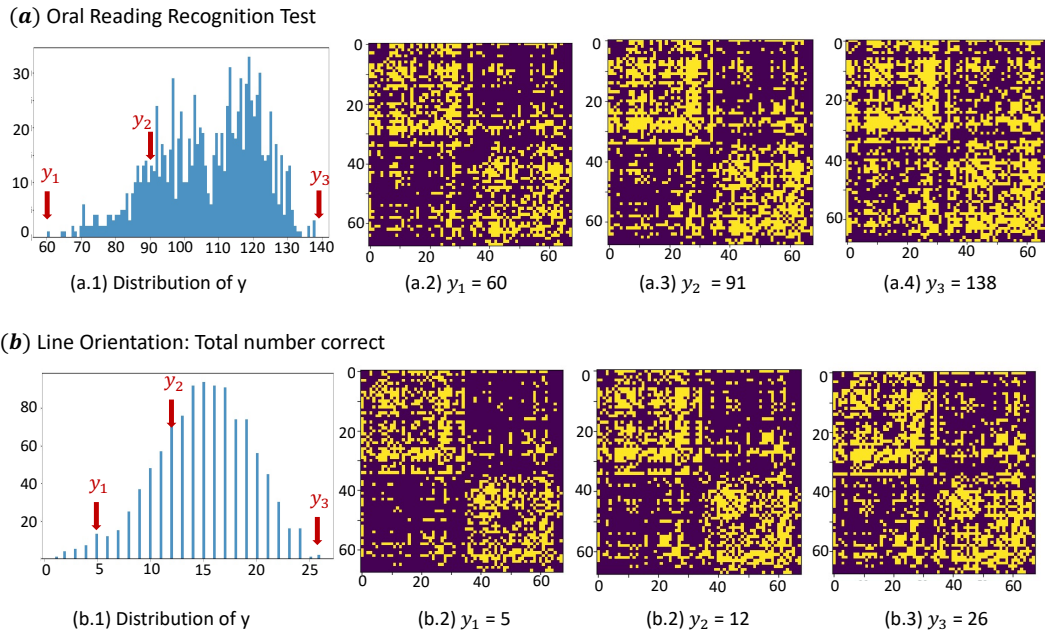


Figure 13: Examples on generating conditional brain networks  $A|y$  for different  $y$ . The first column shows histograms of observed trait scores for the 1065 individuals in HCP. The second to the fourth columns show the means of generated brain networks (after dichotomization) conditional on different  $y$  under the reGATE model.

20) all appear in the top 50 connections. This visual preprocessing center has a few connections (fiber bundles) to the parietal lobe (e.g., regions 7, 24, 28), and then to the frontal lobe. Hence, our results show that richer connections between the visual, sensory, and working memory systems are strongly associated with higher picture vocabulary in both adolescents and adults. Some negative connections within each hemisphere are also observed, although their numbers and strengths are smaller than the positive ones. It is possible that these connections arise from errors introduced during the connection recovery stage or simply statistical noise.

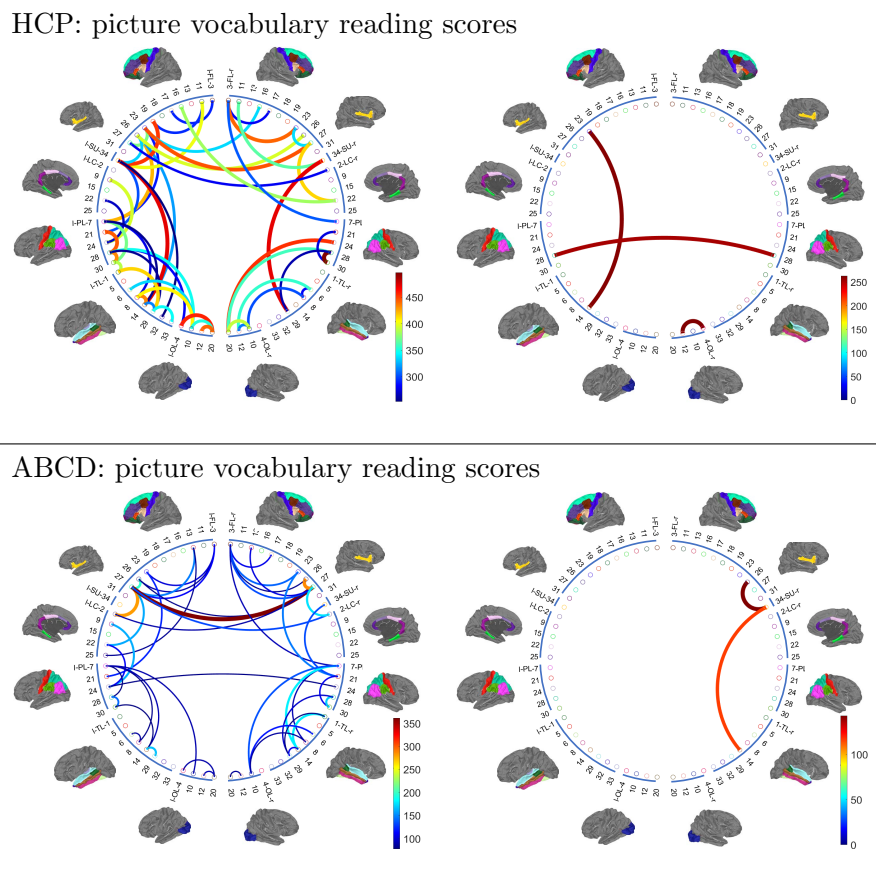


Figure 14: Top 50 pairs of brain regions in terms of the mean changes in the generated brain connectivity between two levels of picture vocabulary reading scores (90% and 10% quantiles). The left panel shows the positive connections among the 50 pairs and the right panel shows negative connections. More details about each node can be found in the Excel spreadsheet in Supplementary Material II.

#### 4.4 Computing details

We summarize the computing details for our analyses of ABCD and HCP data. We run Adam on GATE and reGATE with the learning rate 0.001 on 2 NVIDIA Titan-V GPU. In GATE, we used a

batch size of 128 sampled uniformly at random at each epoch and ran 200 epochs. In reGATE, we used 5-fold CV to calculate the MSE, and ran 100 epochs with batch size of 128 for each training dataset. The latent dimension  $K$  can be chosen as 68 under the same criteria as in Section 3. Table 5 shows the detailed network architectures for the inference model and generative model training.

	Inference model ( $\mu_\phi, \sigma_\phi$ )		Generative model	
	$\mu_\phi$ ( $N = 2$ )	$\sigma_\phi$ ( $N = 2$ )	setting	activation
GATE/reGATE ( $K = 68$ )	$W_{1,\mu} : 68 * 256$ $W_{2,\mu} : 256 * 68$ $b_{1,\mu} : 256 * 1$ $b_{2,\mu} : 68 * 1$ $\varphi_{1,\mu} = \text{Relu}$ $\varphi_{2,\mu} = \text{Linear}$	$W_{1,\sigma} : 68 * 256$ $W_{2,\sigma} : 256 * 68$ $b_{1,\sigma} : 256 * 1$ $b_{2,\sigma} : 68 * 1$ $\varphi_{1,\sigma} = \text{Relu}$ $\varphi_{2,\sigma} = \text{Linear}$	$k$ -NN: 32 $M = 2$ $R = 5$	$h_1$ : Sigmoid $h_2$ : Sigmoid

Table 5: Experimental details and network architectures.  $K$  is the dimension of  $z_i$ ,  $N$  is the number of layers in the inference network,  $M$  is the number of layers in GCN,  $R$  is the dimension of  $X^{(i)}$ .

## 5 Discussion

We develop a novel nonlinear latent factor model to characterize the population distribution of brain connectomes across individuals and depending on human traits. GATE outputs two layers of low dimensional nonlinear latent representations: one on the individuals that can be used as a summary score for visualization and prediction of human traits of interest; and one on the nodes for characterizing the network structure of each individual based on a latent space model. A supervised model reGATE is proposed to analyze the relationship between human traits and brain connectomes. GATE/reGATE are developed based on a deep neural network framework and implemented via a stochastic variational Bayesian algorithm. The algorithm is computationally efficient and can be applied to massive networks with large number of nodes (brain ROIs).

With applications to the ABCD and HCP data, we used GATE and reGATE to study the relationship between brain structural connectomes and various cognition measures. Using the generative model of reGATE, we can simulate brain networks for a given  $y$  (e.g., cognition measure) and compare these brain connectomes and related network topological summaries under different cognition levels while allowing variability across individuals. For these cognition traits, we clearly observe that cross hemispheres connections are important. In the ABCD and HCP datasets, we found that the network density increases while the average path length decreases as the cognition level increases; these network measures for adolescents evaluated in ABCD have a higher variation

than adults in HCP. ReGATE had superior performance in predicting trait scores from brain networks, with the gain particularly notable in the larger ABCD study.

In the future, we would like to extend GATE/reGATE in the following directions. First, in brain networks, a refined division of the brain can give a larger number of nodes, providing a more detailed description of the brain. GATE and reGATE provide a new set of tools for handling high-resolution brain networks, and it becomes interesting to extend the methodology to handle multiresolution data. Moreover, current large studies all collect both functional MRI and diffusion MRI data. It is straightforward to extend GATE/reGATE to jointly embed both functional and structural connectomes, even allowing the strength and nature of the link to vary across individuals and with traits.

### **Acknowledgements**

Data used in the preparation of this article were obtained from the Human Connectome Project (<https://www.humanconnectome.org/>) and Adolescent Brain Cognitive Development (ABCD) Study (<https://abcdstudy.org>). The HCP WU-Minn Consortium (Principal Investigators: David Van Essen and Kamil Ugurbil; 1U54MH091657) were funded by the 16 NIH Institutes and Centers that support the NIH Blueprint for Neuroscience Research; and by the McDonnell Center for Systems Neuroscience at Washington University. The ABCD study is supported by the National Institutes of Health and additional federal partners under award numbers U01DA041022, U01DA041028, U01DA041048, U01DA041089, U01DA041106, U01DA041117, U01DA041120, U01DA041134, U01DA041148, U01DA041156, U01DA041174, U24DA041123, U24DA041147, U01DA041093, and U01DA041025. A full list of supporters is available at <https://abcdstudy.org/federal-partners.html>. A listing of participating sites and a complete listing of the study investigators can be found at <https://abcdstudy.org/scientists/workgroups/>. ABCD consortium investigators designed and implemented the study and/or provided data but did not necessarily participate in the analysis or writing of this report. This manuscript reflects the views of the authors and may not reflect the opinions or views of the NIH or ABCD consortium investigators.

Dunson and Zhang want to acknowledge support from the National Institutes of Health (NIH) of the United States under award number MH118927. We also want to acknowledge the support from the NVIDIA Corporation with their donation of the Titan-V GPU.

## **References**

- Barabási, A.-L. and R. Albert (1999). Emergence of scaling in random networks. *Science* 286(5439), 509–512.
- Binder, J. R., J. A. Frost, T. A. Hammeke, R. W. Cox, S. M. Rao, and T. Prieto (1997). Human brain

- language areas identified by functional magnetic resonance imaging. *Journal of Neuroscience* 17(1), 353–362.
- Boisgueheneuc, F. d., R. Levy, E. Volle, M. Seassau, H. Duffau, S. Kinkingnehun, Y. Samson, S. Zhang, and B. Dubois (2006). Functions of the left superior frontal gyrus in humans: a lesion study. *Brain* 129(12), 3315–3328.
- Bullmore, E. and O. Sporns (2009). Complex brain networks: graph theoretical analysis of structural and functional systems. *Nature Reviews Neuroscience* 10(3), 186.
- Casey, B., T. Cannonier, M. I. Conley, A. O. Cohen, D. M. Barch, M. M. Heitzeg, M. E. Soules, T. Teslovich, D. V. Dellarco, H. Garavan, and C. Orr (2018). The adolescent brain cognitive development (ABCD) study: imaging acquisition across 21 sites. *Developmental Cognitive Neuroscience*.
- Craddock, R. C., S. Jbabdi, C.-G. Yan, J. T. Vogelstein, F. X. Castellanos, A. Di Martino, C. Kelly, K. Heberlein, S. Colcombe, and M. P. Milham (2013). Imaging human connectomes at the macroscale. *Nature Methods* 10(6), 524–539.
- Desikan, R. S., F. Ségonne, B. Fischl, B. T. Quinn, B. C. Dickerson, D. Blacker, R. L. Buckner, A. M. Dale, R. P. Maguire, B. T. Hyman, M. S. Albert, and R. J. Killiany (2006). An automated labeling system for subdividing the human cerebral cortex on MRI scans into gyral based regions of interest. *NeuroImage* 31(3), 968 – 980.
- Durante, D. and D. B. Dunson (2018). Bayesian inference and testing of group differences in brain networks. *Bayesian Analysis* 13(1), 29–58.
- Durante, D., D. B. Dunson, and J. T. Vogelstein (2017). Nonparametric bayes modeling of populations of networks. *Journal of the American Statistical Association* 112(520), 1516–1530.
- Fornito, A., A. Zalesky, and M. Breakspear (2013). Graph analysis of the human connectome: promise, progress, and pitfalls. *NeuroImage* 80, 426–444.
- Friederici, A. D. (2002). Towards a neural basis of auditory sentence processing. *Trends in cognitive sciences* 6(2), 78–84.
- Gelman, A., J. B. Carlin, H. S. Stern, D. B. Dunson, A. Vehtari, and D. B. Rubin (2013). *Bayesian Data Analysis*. Chapman and Hall/CRC.
- Gershon, R. C., M. V. Wagster, H. C. Hendrie, N. A. Fox, K. F. Cook, and C. J. Nowinski (2013). NIH toolbox for assessment of neurological and behavioral function. *Neurology* 80(11), S2–S6.

- Girard, G., K. Whittingstall, R. Deriche, and M. Descoteaux (2014). Towards quantitative connectivity analysis: reducing tractography biases. *NeuroImage* 98, 266 – 278.
- Glasser, M. F., S. M. Smith, D. S. Marcus, J. L. Andersson, E. J. Auerbach, T. E. Behrens, T. S. Coalson, M. P. Harms, M. Jenkinson, S. Moeller, E. C. Robinson, S. N. Sotiropoulos, J. Xu, E. Yacoub, K. Ugurbil, and D. C. Van Essen (2016). The human connectome project’s neuroimaging approach. *Nature Neuroscience* 19(9), 1175–1187.
- Goodfellow, I., Y. Bengio, and A. Courville (2016). *Deep learning*. MIT press.
- Hamilton, W., Z. Ying, and J. Leskovec (2017). Inductive representation learning on large graphs. *Advances in Neural Information Processing Systems*.
- Heaton, R. K., N. Akshoomoff, D. Tulskey, D. Mungas, S. Weintraub, S. Dikmen, J. Beaumont, K. B. Casaletto, K. Conway, J. Slotkin, and R. Gershon (2014). Reliability and validity of composite scores from the nih toolbox cognition battery in adults. *Journal of the International Neuropsychological Society: JINS* 20(6), 588.
- Hinton, G., L. Deng, D. Yu, G. Dahl, A.-r. Mohamed, N. Jaitly, A. Senior, V. Vanhoucke, P. Nguyen, B. Kingsbury, and B. Kingsbury (2012). Deep neural networks for acoustic modeling in speech recognition. *IEEE Signal Processing Magazine* 29.
- Hoff, P. D., A. E. Raftery, and M. S. Handcock (2002). Latent space approaches to social network analysis. *Journal of the American Statistical Association* 97(460), 1090–1098.
- Hoffman, M. D., D. M. Blei, C. Wang, and J. Paisley (2013). Stochastic variational inference. *The Journal of Machine Learning Research* 14(1), 1303–1347.
- Johnson, D. B. (1977). Efficient algorithms for shortest paths in sparse networks. *Journal of the ACM (JACM)* 24(1), 1–13.
- Jones, D. K., T. R. Knosche, and R. Turner (2013, Jun). White matter integrity, fiber count, and other fallacies: the do’s and don’ts of diffusion MRI. *NeuroImage* 73, 239–254.
- Jordan, M. I., Z. Ghahramani, T. S. Jaakkola, and L. K. Saul (1999). An introduction to variational methods for graphical models. *Machine Learning* 37(2), 183–233.
- Kawahara, J., C. J. Brown, S. P. Miller, B. G. Booth, V. Chau, R. E. Grunau, J. G. Zwicker, and G. Hamarneh (2017). Brainnetcnn: Convolutional neural networks for brain networks; towards predicting neurodevelopment. *NeuroImage* 146, 1038–1049.

- Kingma, D. P. and J. Ba (2015). Adam: A method for stochastic optimization. *International Conference on Learning Representations (ICLR)*.
- Kingma, D. P. and M. Welling (2014). Auto-encoding variational bayes. *In International Conference on Learning Representations (ICLR)*.
- Kipf, T. N. and M. Welling (2017). Semi-supervised classification with graph convolutional networks. *In International Conference on Learning Representations*.
- Krizhevsky, A., I. Sutskever, and G. E. Hinton (2012). Imagenet classification with deep convolutional neural networks. *Advances in Neural Information Processing Systems*.
- Ktena, S. I., S. Parisot, E. Ferrante, M. Rajchl, M. Lee, B. Glocker, and D. Rueckert (2018). Metric learning with spectral graph convolutions on brain connectivity networks. *NeuroImage 169*, 431–442.
- Maier-Hein, K. H., P. F. Neher, J.-C. Houde, M.-A. Côté, E. Garyfallidis, J. Zhong, M. Chamberland, F.-C. Yeh, Y.-C. Lin, Q. Ji, and W. Reddick (2017). The challenge of mapping the human connectome based on diffusion tractography. *Nature Communications 8*(1), 1349.
- Miller, K. L., F. Alfaro-Almagro, N. K. Bangerter, D. L. Thomas, E. Yacoub, J. Xu, A. J. Bartsch, S. Jbabdi, S. N. Sotiropoulos, J. L. Andersson, and L. Griffanti (2016). Multimodal population brain imaging in the UK Biobank prospective epidemiological study. *Nature Neuroscience 19*(11), 1523.
- Nowicki, K. and T. A. B. Snijders (2001). Estimation and prediction for stochastic blockstructures. *Journal of the American Statistical Association 96*(455), 1077–1087.
- Park, H.-J. and K. Friston (2013). Structural and functional brain networks: from connections to cognition. *Science 342*(6158), 1238411.
- Rezende, D. J., S. Mohamed, and D. Wierstra (2014). Stochastic backpropagation and approximate inference in deep generative models. *In International Conference on Machine Learning*, 1278–1286.
- Sermanet, P., S. Chintala, and Y. LeCun (2012). Convolutional neural networks applied to house numbers digit classification. *In International Conference on Pattern Recognition (ICPR 2012)*.
- Smith, R. E., J. D. Tournier, F. Calamante, and A. Connelly (2012, Sep). Anatomically-constrained tractography: improved diffusion MRI streamlines tractography through effective use of anatomical information. *NeuroImage 62*(3), 1924–1938.

- Tuch, D. S. (2004, Dec). Q-ball imaging. *Magn Reson Med* 52(6), 1358–1372.
- Van der Maaten, L. and G. Hinton (2008). Visualizing data using t-sne. *Journal of machine learning research* 9(11).
- Van Essen, D. C., S. M. Smith, D. M. Barch, T. E. Behrens, E. Yacoub, K. Ugurbil, and W.-M. H. Consortium (2013). The WU-Minn human connectome project: an overview. *NeuroImage* 80, 62–79.
- Van Essen, D. C., K. Ugurbil, E. Auerbach, D. Barch, T. Behrens, R. Bucholz, A. Chang, L. Chen, M. Corbetta, S. W. Curtiss, and S. Della Penna (2012). The human connectome project: a data acquisition perspective. *NeuroImage* 62(4), 2222–2231.
- Wang, L., Z. Zhang, and D. B. Dunson (2019). Symmetric bilinear regression for signal subgraph estimation. *IEEE Transactions on Signal Processing* 67, 1929–1940.
- Watts, D. J. and S. H. Strogatz (1998). Collective dynamics of ‘small-world’ networks. *Nature* 393(6684), 440.
- Yoo, Y., S. Yun, H. Jin Chang, Y. Demiris, and J. Young Choi (2017). Variational autoencoded regression: high dimensional regression of visual data on complex manifold. In *Proceedings of the IEEE Conference on Computer Vision and Pattern Recognition*, pp. 3674–3683.
- Zhang, L. W. Z. and D. Dunson (2019). Common and individual structure of multiple networks. *The Annals of Applied Statistics* 13(1), 85–112.
- Zhang, Z., G. I. Allen, H. Zhu, and D. Dunson (2019). Tensor network factorizations: Relationships between brain structural connectomes and traits. *NeuroImage* 197, 330–343.
- Zhang, Z., M. Descoteaux, J. Zhang, G. Girard, M. Chamberland, D. Dunson, A. Srivastava, and H. Zhu (2018). Mapping population-based structural connectomes. *NeuroImage* 172, 130 – 145.
- Zhou, H., L. Li, and H. Zhu (2013). Tensor regression with applications in neuroimaging data analysis. *Journal of the American Statistical Association* 108(502), 540–552.

## SUPPLEMENTARY MATERIAL

### Auto-encoding brain networks with application to analyzing large-scale brain imaging datasets

In this Supplement, we list the detailed neural network modeling framework for GATE/reGATE, and describe additional numerical studies.

#### S.1 Parameter setup in $q_\phi(z_i | A_i)$ defined in Equation (2.12) for GATE

In Section 2.2.4, we aim to approximate  $p_\theta(z_i | A_i)$  by  $q_\phi(z_i | A_i)$ , where  $q_\phi(z_i | A_i) \sim N(\mu_\phi, \sigma_\phi^2)$ . Particularly, we learn  $\mu_\phi$  and  $\sigma_\phi^2$  via

$$\begin{aligned} \mu_\phi(A_i) &= \varphi_{N,\mu}[W_{N,\mu}\varphi_{N-1,\mu}\{W_{N-1,\mu}\cdots\varphi_{1,\mu}(W_{1,\mu}A_i + b_{1\mu}) + b_{N-1,\mu}\} + b_{N,\mu}], \quad (\text{S.1}) \\ \text{diag}\{\sigma_\phi^2(A_i)\} &= \text{diag}\{\varphi_{N,\sigma}[W_{N,\sigma}\varphi_{N-1,\sigma}\{W_{N-1,\sigma}\cdots\varphi_{1,\sigma}(W_{1,\sigma}A_i + b_{1\sigma}) + b_{N-1,\sigma}\} + b_{N,\sigma}]\}, \end{aligned}$$

where  $b_{i,\mu}, W_{i,\mu}, b_{i,\sigma}, W_{i,\sigma}$  for  $i = 1, \dots, N$  are weights within the deep neural networks,  $N$  is the number of layers that determine the model's learning capacity, and  $\{\varphi_{i,\mu}\}, \{\varphi_{i,\sigma}\}$  are activation functions that will be specified later. We denote these weights and activation functions together as the parameter  $\phi$ .

#### S.2 Derivation of the evidence lower bound in GATE

In this part, we show how the difference between  $\log p_\theta(A_i)$  and  $D_{KL}(q_\phi(z_i|A_i)||p_\theta(z_i|A_i))$  can be expressed as the evidence lower bound in equation (2.13). Note that

$$\begin{aligned} & D_{KL}(q_\phi(z_i|A_i)||p_\theta(z_i|A_i)) \\ &= \int q_\phi(z_i|A_i) \log \frac{q_\phi(z_i|A_i)}{p_\theta(z_i|A_i)} dz_i = \int q_\phi(z_i|A_i) \log \frac{q_\phi(z_i|A_i)p_\theta(A_i)}{p_\theta(A_i|z_i)p_\theta(z_i)} dz_i \\ &= \log p_\theta(A_i) + D_{KL}(q_\phi(z_i|A_i)||p_\theta(z_i)) - \mathbb{E}_{q_\phi(z_i|A_i)} (\log p_\theta(A_i|z_i)). \end{aligned}$$

Then we have

$$\begin{aligned} & \log p_\theta(A_i) - D_{KL}(q_\phi(z_i|A_i)||p_\theta(z_i|A_i)) \\ &= \mathbb{E}_{q_\phi(z_i|A_i)} [\log p_\theta(A_i|z_i)] - D_{KL}(q_\phi(z_i|A_i)||p_\theta(z_i)) := -\mathcal{L}(A_i; \theta, \phi). \quad (\text{S.2}) \end{aligned}$$

### S.3 Derivation of the evidence lower bound (ELBO) in reGATE objective function

In this part, we derive the ELBO from the joint log-likelihood of  $(A_i, y_i)$  in equation (S.3). Let  $y_i$  be the trait of the  $i$ -th subject. The joint log likelihood of  $(A_i, y_i)$  can be expressed as

$$\begin{aligned}
\log p_\theta(A_i, y_i) &= \mathbb{E}_{q_\phi(z_i|A_i)} \log \frac{p_\theta(A_i, z_i)p_\theta(y_i|A_i, z_i)}{p_\theta(z_i|A_i, y_i)} \\
&= \mathbb{E}_{q_\phi(z_i|A_i)} \log \frac{p_\theta(A_i|z_i)p_\theta(z_i)p_\theta(y_i|z_i)q_\phi(z_i|A_i)}{q_\phi(z_i|A_i)p_\theta(z_i|y_i, A_i)} \\
&= \mathbb{E}_{q_\phi(z_i|A_i)} \log p_\theta(y_i|z_i) + \mathbb{E}_{q_\phi(z_i|A_i)} \log p_\theta(A_i|z_i) - D_{KL}(q_\phi(z_i|A_i)||p_\theta(z_i)) \\
&\quad + D_{KL}(q_\phi(z_i|A_i)||p_\theta(z_i|y_i, A_i)) \\
&= -\mathcal{L}(A_i, y_i; \theta, \phi) + D_{KL}(q_\phi(z_i|A_i)||p_\theta(z_i|y_i, A_i)), \tag{S.3}
\end{aligned}$$

where we have  $p_\theta(y_i|A_i, z_i) = p_\theta(y_i|z_i)$  since we assume the human trait  $y_i$  and the brain connectivity  $A_i$  are conditionally independent given the latent representation  $z_i$  for the  $i$ -th subject.

### S.4 Approximation of the ELBO in reGATE objective

Similar to Section 2.2.4, we form the Monte Carlo estimate of  $\mathcal{L}(A_i, y_i; \theta, \phi)$  as

$$\begin{aligned}
\mathcal{L}(A_i, y_i; \theta, \phi) &\simeq \tilde{\mathcal{L}}(A_i, y_i; \theta, \phi) \\
&= -\frac{1}{L} \sum_{\ell=1}^L (\log p_\theta(A_i|z_i^\ell) + \log p_\theta(y_i|z_i^\ell)) + \frac{1}{2} \sum_{k=1}^K (\mu_k^2 + \sigma_k^2 - 1 - \log(\sigma_k^2)),
\end{aligned}$$

and estimate  $\theta, \phi$  following the stochastic variational Bayesian Algorithm 1 by replacing  $\tilde{\mathcal{L}}(A_i; \theta, \phi)$  with  $\tilde{\mathcal{L}}(A_i, y_i; \theta, \phi)$ .

### S.5 Derivation of the posterior distribution of $z_i$ given $y_i$

The posterior distribution of  $z_i$  given  $y_i$  can has an explicit expression as follows: To achieve this goal, for each  $y_i$ , we need to learn the posterior distribution of  $A_i | y_i$ . In fact, the posterior computation of  $A_i$  given a particular  $y_i$   $p_\theta(z_i|y_i)$  and  $p_\theta(A_i|z_i)$ , where the latter is learned via the inference model in reGATE. Recall  $p_\theta(z_i) \sim N(0, I_K)$ , and  $p_\theta(y_i|z_i) \sim N(z_i^\top \beta + b, \sigma^2)$ . The posterior

distribution of  $z_i$  given  $y_i$  has an explicit expression as follows:

$$\begin{aligned}
p_\theta(z_i|y_i) &\propto p_\theta(y_i|z_i)p_\theta(z_i) \\
&\propto \exp \left\{ -\frac{(y_i - z_i^\top \beta - b)^2}{2\sigma^2} - \frac{z_i^\top z_i}{2} \right\} \\
&\propto \exp \left\{ -\frac{z_i^\top z_i + z_i^\top \beta \beta^\top z_i / \sigma^2 - 2z_i^\top \beta (y_i - b) / \sigma^2}{2} \right\} \\
&\propto \exp \left\{ -\frac{z_i^\top (I_K + \beta \beta^\top / \sigma^2) z_i - 2z_i^\top \beta (y_i - b) / \sigma^2}{2} \right\}.
\end{aligned}$$

Therefore, we have  $p_\theta(z_i|y_i) \sim N(\mu_z(y_i), \Sigma_z(y_i))$ , where

$$\mu_z(y_i) = (I_K + \beta \beta^\top / \sigma^2)^{-1} \beta (y_i - b) / \sigma^2, \quad \text{and} \quad \Sigma_z(y_i) = (I_K + \beta \beta^\top / \sigma^2)^{-1}. \quad (\text{S.4})$$

## S.6 Additional real data analysis: Data visualization for HCP

Similar to Section 4.1, we first visualize the latent features of each individual’s connectome in HCP, from which we can investigate the relationship between the structural connectivity and the four traits. We train GATE on 1065 brain networks extracted from HCP to obtain low-dimensional representations  $z_i$ . We then plot the posterior mean of  $z_i|A_i$  using t-SNE in  $\mathbb{R}^3$  colored with its corresponding trait score. For each cognition trait, we only plot 200 subjects’ data, 100 subjects with low trait scores and 100 subjects with high scores. Figure 15 (a) – (d) shows the separated map points between the two groups for different traits, and the separation is more significant under the supervised reGATE approach.

We also apply GATE and reGATE to the HCP test-retest data. Figure 16 shows 10 selected subjects, with each unique combination of color and number representing two scans from the same subject. For both unsupervised GATE and supervised reGATE, the test-retest brain networks display a clear clustering pattern, implying that brain networks extracted from repeated scans are reproducible, and we can distinguish between different subjects based on the embedded feature  $z_i$ .

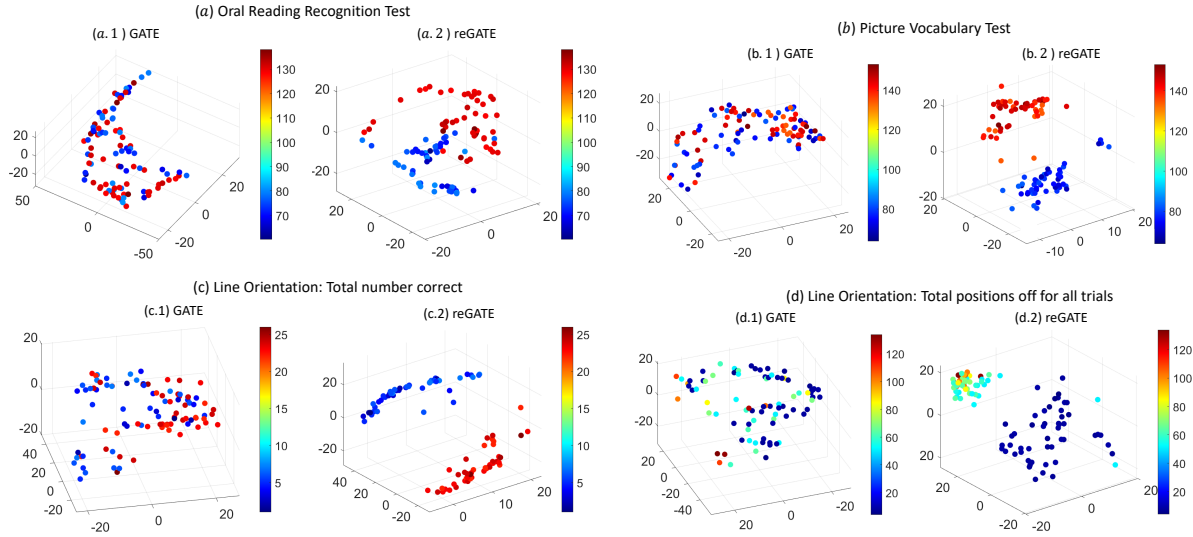


Figure 15: HCP study: visualization of low dimensional embedding  $z_i$  learned from GATE and reGATE. For each trait, we display 100 subjects with the lowest trait scores and 100 subjects with the highest scores. Colors represent the trait scores.

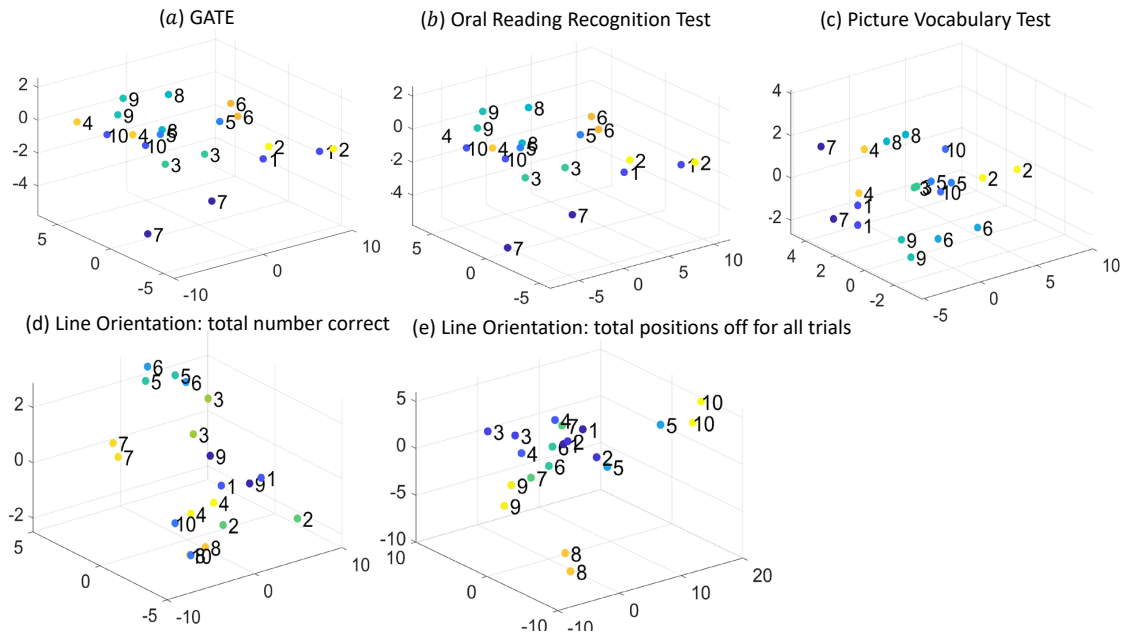


Figure 16: Visualization of low dimensional embedding  $z_i$  from the HCP test-retest data set under GATE and reGATE with four different traits. Each unique combination of color represents two scans from the same subject.